

UBIQUITOUS OUTFLOWS IN DEEP2 SPECTRA OF STAR-FORMING GALAXIES AT Z=1.4

BENJAMIN J. WEINER^{1,2}, ALISON L. COIL^{1,3,4}, JASON X. PROCHASKA⁵, JEFFREY A. NEWMAN⁶, MICHAEL C. COOPER^{1,7}, KEVIN BUNDY⁸, CHRISTOPHER J. CONSELICE⁹, AARON A. DUTTON⁵, S. M. FABER⁵, DAVID C. KOO⁵, JENNIFER M. LOTZ^{10,11}, G.H. RIEKE¹, K.H.R. RUBIN⁵

ApJ in press

ABSTRACT

Galactic winds are a prime suspect for the metal enrichment of the intergalactic medium and may have a strong influence on the chemical evolution of galaxies and the nature of QSO absorption line systems. We use a sample of 1406 galaxy spectra at $z \sim 1.4$ from the DEEP2 redshift survey to show that blueshifted Mg II $\lambda\lambda$ 2796, 2803 Å absorption is ubiquitous in starforming galaxies at this epoch. This is the first detection of frequent outflowing galactic winds at $z \sim 1$. The presence and depth of absorption are independent of AGN spectral signatures or galaxy morphology; major mergers are not a prerequisite for driving a galactic wind from massive galaxies. Outflows are found in coadded spectra of galaxies spanning a range of $30\times$ in stellar mass and $10\times$ in star formation rate (SFR), calibrated from K -band and from MIPS IR fluxes. The outflows have column densities of order $N_H \sim 10^{20} \text{cm}^{-2}$ and characteristic velocities of $\sim 300 - 500$ km/sec, with absorption seen out to 1000 km/sec in the most massive, highest SFR galaxies. The velocities suggest that the outflowing gas can escape into the IGM and that massive galaxies can produce cosmologically and chemically significant outflows. Both the Mg II equivalent width and the outflow velocity are larger for galaxies of higher stellar mass and SFR, with $V_{wind} \sim SFR^{0.3}$, similar to the scaling in low redshift IR-luminous galaxies. The high frequency of outflows in the star-forming galaxy population at $z \sim 1$ indicates that galactic winds occur in the progenitors of massive spirals as well as those of ellipticals. The increase of outflow velocity with mass and SFR constrains theoretical models of galaxy evolution that include feedback from galactic winds, and may favor momentum-driven models for the wind physics.

Subject headings: galaxies: high-redshift — intergalactic medium — galaxies: evolution — ultraviolet: ISM

1. INTRODUCTION

As galaxies form, they accrete gas from infalling objects and from the intergalactic medium (IGM). The process of galaxy formation also is apparently not 100% efficient at getting gas into galaxies, as some galaxies are observed to drive galactic winds or outflows, expelling gas, possibly to escape the galaxy itself. The baryonic mass in local disks compared to their dark matter halo mass is lower than the global value, which may point to past episodes of gas removal by outflows (e.g. Fukugita, Hogan & Peebles 1998; Mo & Mao 2004; Dutton et al. 2007). Galactic winds can be driven by stellar winds, supernovae, or active galactic nuclei; observationally, in local galaxies winds are a general consequence of high star formation rates or star formation surface density (e.g. Lehnert & Heckman 1996). Outflows may play a large role in regulating the baryon and metal content of galaxies, and in enriching the intergalactic medium. The frequency of outflows

and their dependence on host galaxy properties such as mass and star formation rate (SFR) are key ingredients for modeling the evolution of the IGM and the chemical evolution and gas processing of galaxies. Observations of winds and their implications are discussed in the review by Veilleux, Cecil & Bland-Hawthorn (2005).

In nearby galaxies, strong winds driven by supernovae are seen mainly in starbursting dwarfs, starburst galaxies such as M82, and luminous and ultraluminous infrared galaxies (LIRGs and ULIRGs); the latter are frequently mergers and often host active galactic nuclei (AGN). Winds are often found in galaxies above a SFR surface density threshold of $\sim 0.1 M_{\odot} \text{yr}^{-1} \text{kpc}^{-2}$ (Heckman 2002), while large-scale outflows are not seen in local ordinary disk galaxies. The Milky Way has a nuclear wind that would not be detectable outside the Local Group (Veilleux et al. 2005). It is not clear whether a galaxy such as the Milky Way has had a galactic-scale outflow in the past. We do know that the global SFR density was $\sim 10\times$ higher at $z = 1$ than today (e.g. Lilly et al. 1996; Hopkins 2004). Noeske et al. (2007a) showed that the higher SFR is due to higher rates at $z = 1$ in starforming galaxies across a wide mass range, rather than an increased frequency of starbursts in a fraction of galaxies. It is thus possible that a large fraction of the galaxy population drove outflows in the past; that is one question this paper seeks to address.

The dependence of outflows on galaxy mass is also of great interest. Larson (1974) showed that supernova-driven winds could heat and eject interstellar gas during galaxy formation, and that this process could be more effective in smaller galaxies. The influential theoretical treatment of Dekel & Silk (1986) found that winds could remove a significant amount of gas from low-mass galaxies, $V_{vir} \lesssim 100 \text{ km s}^{-1}$, resolving

¹ Steward Observatory, 933 N. Cherry St., University of Arizona, Tucson, AZ 85721

² bjw@as.arizona.edu

³ Hubble Fellow

⁴ Department of Physics, and CASS, University of California, San Diego, La Jolla, CA 92093-0424

⁵ UCO/Lick Observatory, University of California, Santa Cruz, Santa Cruz, CA 95064

⁶ Dept. of Physics and Astronomy, University of Pittsburgh, Pittsburgh, PA 15260

⁷ Spitzer Fellow

⁸ Department of Astronomy and Astrophysics, University of Toronto, Toronto, ON M5S 3H4, CA

⁹ School of Physics and Astronomy, University of Nottingham, Nottingham, UK

¹⁰ National Optical Astronomy Observatories, Tucson, AZ 85719

¹¹ Leo Goldberg Fellow

several issues in cold dark matter galaxy formation. A number of authors have simulated the effect of winds on the ISM, e.g. Mac Low & Ferrara (1999). Their simulations suggested that winds do not entirely clear ISM gas except at extremely low masses, but that they are efficient at preferentially ejecting metals. However, other treatments of wind physics suggest that winds in massive galaxies in a high-SFR phase could limit the SFR and eject a substantial amount of gas (Murray, Quataert & Thompson 2005). The physical conditions in the wind fluid and the mass-loading of cold gas into the hot wind are quite difficult to constrain from observations (e.g. Strickland & Stevens 2000; Murray et al. 2005). It remains open whether metals are ejected and the IGM enriched preferentially by low or high mass galaxies, and the degree to which AGN-driven winds contribute.

Fossil evidence of the effect of winds comes from studies of the mass-metallicity relation in local samples and in the Sloan Digital Sky Survey. These studies show that low-mass galaxies have low effective yields, indicating that winds have removed metals from them; the behavior of the effective yield is evidence for past winds in galaxies of stellar mass $M_* < 10^{10} M_\odot$ (Garnett 2002; Tremonti et al. 2004). Dalcanton (2007) showed that star formation after an outflow episode is efficient at returning the measured metal yield to its nominal value. Therefore, winds must preferentially carry away enriched gas to reduce the yield in low-mass, high gas-fraction galaxies. However, because even enriched outflows will not substantially change the observed effective yield in high-mass galaxies, the observations do not rule out winds at higher masses (Tremonti et al. 2004). The behavior of the effective yield does not provide evidence either for or against past winds in high mass galaxies.

Direct evidence for galactic winds in the local universe comes from a variety of observations including X-rays, the morphology and kinematics of interstellar emission lines, and outflow kinematics in interstellar absorption lines (Veilleux et al. 2005 and references therein). Blueshifted absorption lines are the wind signatures that are most straightforward to observe and interpret in distant galaxies, and the method we use in this paper.

In local galaxies, Phillips (1993) found blueshifted Na I absorption spread across the disk of the starforming galaxy NGC 1808, associated with extraplanar dust plumes. Blueshifted Na I absorption was observed in 12 of 18 infrared-luminous starburst galaxies (Heckman et al. 2000), with outflow velocities of 100–600 km s⁻¹. Further surveys have confirmed that blueshifted Na I absorption is common in IR-bright starburst galaxies (Rupke, Veilleux & Sanders 2002, 2005a,b; Martin 2005, 2006) and is also found in dwarf starbursts (Schwartz & Martin 2004). Low-ionization UV lines behave similarly to the Na I lines (Schwartz et al. 2006).

Tremonti, Moustakas & Diamond-Stanic (2007) detected blueshifted absorption in Mg II in $z \sim 0.6$ very luminous post-starburst galaxies. The outflow velocities are very large, 500–2000 km s⁻¹, leading them to suggest these are relics of AGN-driven outflows. Sato et al. (2008) have found blueshifted Na I absorption in red-sequence galaxies at $z \sim 0.4$ in the DEEP2 survey; they find a higher frequency of outflows at greater infrared luminosity, but also find some outflows in quiescent galaxies that show signs of being post-starbursts.

At high redshift, $z \sim 3$, outflows with typical velocities of 250 km s⁻¹ are found in rapidly starforming galaxies selected by the Lyman-break technique. The gravitationally lensed

galaxy cB58 (Pettini et al. 2000, 2002) and the composite spectrum of a large sample of Lyman-break galaxies (Shapley et al. 2003) show blueshifted outflows in both low- and high-ionization UV interstellar lines such as Si II and C IV. These early, rapidly starforming galaxies are commonly thought to be progenitors of today’s massive ellipticals (e.g. Adelberger et al. 2005), although this point remains controversial (e.g. Conroy et al. 2008). At $z > 3$, Lyman- α emitting galaxies also exhibit blueshifted absorption and Ly- α red wings that could arise in outflows (Frye et al. 2002; Dawson et al. 2002; Sawicki et al. 2008). AGN also drive high-velocity outflows (e.g. Morganti et al. 2005; Nesvadba et al. 2006; Trump et al. 2006); these might affect the host galaxy ISM. The increased frequency of AGN and QSOs at high redshift could have a significant effect on subsequent galaxy evolution, although the efficiency of coupling an AGN outflow to the galactic ISM is not well understood.

In summary, at low redshift we know that galaxies with high SFR surface density have outflows, and at least some post-starbursts also do. At high redshift, galaxies selected by methods that find high SFRs show outflows, but following the destiny of these progenitors to the present day is uncertain.

In this work we investigate Mg II absorption in star-forming galaxies with spectra from the DEEP2 redshift survey (Davis et al. 2003), which reach Mg II at $z \sim 1.4$. Mg II absorption probes cool, atomic gas (neutral gas and H II with metals in low ionization states), as does Na I; Mg II has an ionization potential of 15.0 eV while Na I is 5.1 eV, so Mg II is less easily photodissociated and suffers smaller ionization corrections. The Mg II line has not been used to probe galactic-scale or star-formation driven outflows prior to Tremonti et al. (2007), mostly due to its location in the near-UV. Mg II outflows are seen in a small fraction of Seyfert nuclei (Crenshaw et al. 1999) and in low-ionization broad absorption line QSOs (LoBALs, which are $\sim 1\%$ of QSOs; Trump et al. 2006). Mg II has been used in many studies of QSO absorption systems at intermediate redshift; these show that strong Mg II systems ($EW > 0.3 \text{ \AA}$) occur within a few tens of kpc of luminous galaxies (e.g. Lanzetta & Bowen 1990; Bergeron & Boisse 1991; Steidel, Dickinson & Persson 1994). Possible sources of these Mg II systems include extended rotating gas, tidal debris, associated clustered absorption, and outflows (e.g. Charlton & Churchill 1998; Steidel et al. 2002; Bouché et al. 2006; Kaprczak et al. 2007; Tinker & Chen 2008; Wild et al. 2008).

Here, we use co-added spectra of 1406 galaxies at $z = 1.28$ to 1.5 from the DEEP2 survey to detect low-ionization outflowing gas in absorption lines of Mg II 2796, 2803 Å and Mg I 2852 Å. We find absorption strengths of this low-ionization gas comparable to strong Mg II QSO absorption systems. The characteristic outflow velocities are of order 300–500 km s⁻¹. We use *K*-band and Spitzer/MIPS 24 μm data for part of the sample to calibrate stellar mass and star formation rate estimates, and explore the dependence of outflows on mass and SFR.

We assume a Λ CDM cosmology with $H_0 = 70$, $\Omega_m = 0.3$, and $\Omega_\Lambda = 0.7$. Magnitudes in this paper are in the AB system unless otherwise noted, and wavelengths at $> 2000 \text{ \AA}$ are given in air, although the reduction was done on vacuum wavelengths.

We describe the sample of galaxies and spectroscopy in Section 2. Section 3 presents the composite spectrum and introduces the evidence for outflows in Mg II absorption, while

Section 4 analyzes and quantifies the outflow component of Mg II. In Section 5 we compute restframe properties of the host galaxies and in section 6 we measure the dependence of outflows on the host galaxy properties. Section 7 analyzes the observations, including the physical properties of the outflow and the implications for wind models, and 8 summarizes the conclusions. The key results of the paper are found in Sections 3, 6 and 7.

2. SAMPLE AND DATA EXTRACTION

2.1. Spectroscopic data and sample selection

The sample of galaxies we study is drawn from the DEEP2 galaxy redshift survey (Deep Extragalactic Evolutionary Probe 2; Davis et al. 2003). DEEP2 is selected from *BRI* imaging with the CFHT CFH12K camera (Coil et al. 2004b), and has obtained redshifts for approximately 32,000 galaxies, using the DEIMOS spectrograph at the Keck II telescope. The DEEP2 sample is distributed across four fields and is selected to have $18.5 < R_{AB} < 24.1$. In three of the four fields, a color selection in $B - R, R - I$ is applied to exclude galaxies at $z < 0.7$ (Coil et al. 2004a), which does not affect the high-redshift subsample we use in this paper. The fourth field, the Extended Groth Strip, allows testing the color selection and confirms that the excluded galaxies are at $z < 0.7$.

DEEP2 DEIMOS spectra are taken with a 1200 lines/mm grating and 1.0" slit, yielding resolution $R \sim 5000$ and a scale of 0.33 Å/pixel. A typical DEEP2 spectrum has wavelength coverage $\sim 6600 - 9100$ Å; the exact limits vary depending on the object's location on the slit mask. Galaxy spectra are reduced by an automated pipeline, extracted to 1-d in a window that is typically 1.5 times the spatial FWHM of the object along the slit, and processed by an automated template fitter to determine a set of candidate redshifts. The program fits a linear combination of an artificial emission-line template containing [O II], H β , [O III], and H α , and an early type galaxy template derived from the SDSS Luminous Red Galaxy sample (Eisenstein et al. 2001), shifting the templates relative to the spectrum and computing χ^2 . It finds minima in χ^2 and nominates these as candidate redshifts. The program also attempts to fit stellar and QSO templates.

Each spectrum is then examined by a member of the DEEP2 team to select the correct redshift or reject the redshift as unconfirmed. To be accepted as a confirmed redshift, a galaxy must show at least two spectral features. The DEIMOS spectra resolve the [O II] $\lambda\lambda$ 3726, 3729 Å doublet and a detection of both lines counts as two features. For galaxies at $0.8 < z < 1.5$, [O II] emission is the primary redshift indicator in DEEP2. Beyond $z \sim 1.5$, [O II] is increasingly difficult to detect in the OH airglow line forest, so the DEEP2 wavelength range was chosen to only extend as far as [O II] at $z = 1.5$.

To study the properties of the Mg II near-UV absorption doublet at $\lambda\lambda$ 2795.53, 2802.71 Å, we selected DEEP2 spectra of confirmed galaxies that have wavelength coverage reaching to 2788.7 Å in the restframe ($-730, -1500$ km/sec relative to Mg II 2795.53, 2802.71 Å), or bluer. The limited wavelength coverage of DEEP2 spectra and the requirement of [O II] to measure an accurate redshift mean that this sample is limited to galaxies at the highest redshifts in DEEP2, $z \sim 1.4$, where [O II] is detected and Mg II is in the DEEP2 spectrum. At $z = 1.4$, Mg II is observed at ~ 6720 Å and [O II] is at ~ 8950 Å. Bluer UV absorption lines such as Fe II or C IV cannot be measured with these data. A small number

of objects with $z > 1.5$ also meet the wavelength coverage criterion, but objects with $z > 1.5$ in DEEP2 are generally QSOs identified by UV emission, so we excluded all objects with $z > 1.5$.

From a catalog with 32,308 confirmed galaxy and QSO redshifts, these criteria select 1409 unique objects at $z < 1.5$. Three are AGN/QSOs with strong broad Mg II emission, identified in the DEEP2 catalog as CLASS=AGN, and we exclude them. The 1406 galaxies are hereafter called the Mg II sample. 31 of the galaxies were observed twice, and we used only the first observation. All 1406 galaxies have broadband *BRI* magnitudes from the CFHT CFH12K observations. The median redshift of the 1406-galaxy sample is 1.379 and the 5%-95% range is 1.314 – 1.451. The DEEP2 survey is selected at *R*-band, so at $z \sim 1.4$ it is effectively selected at restframe 2800 Å. Therefore the sample strongly favors star-forming galaxies in the “blue cloud” of the bimodal galaxy color-magnitude diagram (Weiner et al. 2005; Willmer et al. 2006).

From comparing the measurements of 1453 galaxies in the entire DEEP2 sample that were observed twice, the errors on a single redshift measurement are $\sigma(z) = 1.3 \times 10^{-4}$ and 5.4×10^{-4} at 68% and 95% probability respectively. The errors on relative velocity are $\sigma(v) = c\sigma(z)/(1+z)$, yielding 16 and 68 km s $^{-1}$ at 68% and 95%, at $z = 1.4$. In this paper, we are concerned with the velocity of Mg II relative to a systemic velocity measured at [O II]. Since these are at the extreme blue and red ends of the DEEP2 spectrum, the relative velocity requires a good global wavelength calibration. We tested this empirically by comparing the relative velocities of [O II] 3727 and [O III] 5007 for galaxies with both lines, at $z \sim 0.8$ where they are at blue and red ends of the DEEP2 spectrum. In 3772 galaxies, the median offset is 0.9 km s $^{-1}$ and the 68% and 95% ranges are ± 36 and ± 169 km s $^{-1}$ respectively. Outliers are caused in part by errors in the emission line fitting due to sky residuals and weak-emission objects, so the actual wavelength scale is better. These 1σ redshift and wavelength accuracies are considerably smaller than the few hundred km s $^{-1}$ outflow offsets we show to be typical in the Mg II sample.

2.2. Co-addition of DEEP2 spectra

The median signal to noise of DEEP2 spectra in the Mg II sample near 2820 Å restframe is 0.55 per pixel, or 1.1 per FWHM. The typical exposure time of 1 hour is designed for acceptable detection of nebular emission lines, but does not yield S/N/pixel high enough to study absorption lines in detail in most of the objects. We construct a high S/N composite by co-adding spectra in their rest frame.

We co-add the spectra using an IDL routine written by members of the DEEP2 team. From an input catalog of DEEP2 galaxies, the routine collects their 1-D extracted spectra, corrects each for telluric absorption, shifts the wavelength scale to the rest frame based on the DEEP2 catalog redshift, which is derived from [O II] in these objects, and coadds the spectra, weighting at each pixel by the inverse variance.

Weighting solely by the inverse variance would mean that bright objects contribute super-linearly to the coadd, since they have higher flux and lower variance. For the present sample, for each spectrum we renormalized the inverse variance array so that it has median of 1, prior to the telluric correction. The effect is to retain the dependence of the inverse variance on wavelength in each individual spectrum, e.g. due to night

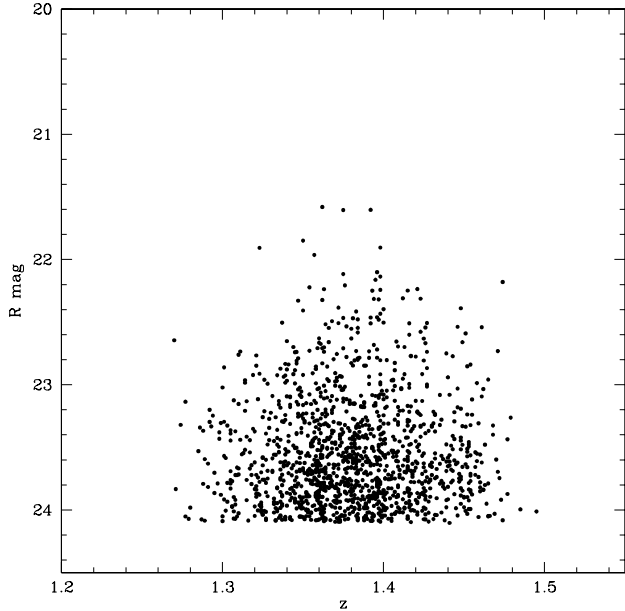


FIG. 1.— Redshift and R magnitude of the 1406 galaxies in the Mg II sample. The redshift limits are set by the wavelength coverage of DEEP2 and $R = 24.1$ is the DEEP2 magnitude selection limit.

sky lines, but to take out the object-to-object difference, to avoid weighting bright galaxies more due to the higher S/N of their spectra. The coadded spectrum is light-weighted, not equal-number-weighted, across the galaxy sample. We did not flux-calibrate the spectra prior to coaddition; since the galaxies occupy a narrow redshift range, the instrumental response does not vary greatly in the pixels contributing to a given rest wavelength. The pixel spacing in the coadded spectrum is 13.8 km s^{-1} at 2800 \AA . The S/N/pixel in the coadded spectrum of 1406 galaxies is 21, and in the subsamples of Section 6 the S/N/pixel is 8 to 14.

3. MG II ABSORPTION IN DEEP2 GALAXIES

3.1. The coadded spectrum at $z = 1.4$

Figure 2 shows the full coadded spectrum of the 1406-galaxy Mg II sample. The spectrum is dominated by strong [O II] 3727 emission. There are prominent Balmer absorption lines indicating a young stellar population with A stars, [Ne III] 3869 emission, and some narrow Balmer emission. The UV spectrum blueward of [O II] is relatively featureless except for weak He I 3188 \AA emission, and strong absorption from Mg I at 2852 \AA and the Mg II doublet at 2796, 2803 \AA .

In Figure 3 we extract the regions of the co-added spectrum around the lines [O II] 3726.0, 3728.8 \AA , Mg II 2795.5, 2802.7 \AA , and Mg I 2852.1 \AA , and plot them on restframe velocity scales derived from the DEEP2 catalog redshift. At this high redshift, the DEEP2 redshift is based solely on fitting [O II]. The [O II] doublet is thus necessarily fixed to zero velocity, here referenced to the redder line at 3728.82 \AA . The immediately visible result is that the Mg II and Mg I absorption lines are asymmetric and blueshifted by a few hundred km s^{-1} with respect to the systemic velocity defined by [O II].

The lines of the [O II] doublet are symmetric, with low-intensity wings more extended than Gaussian. The wings

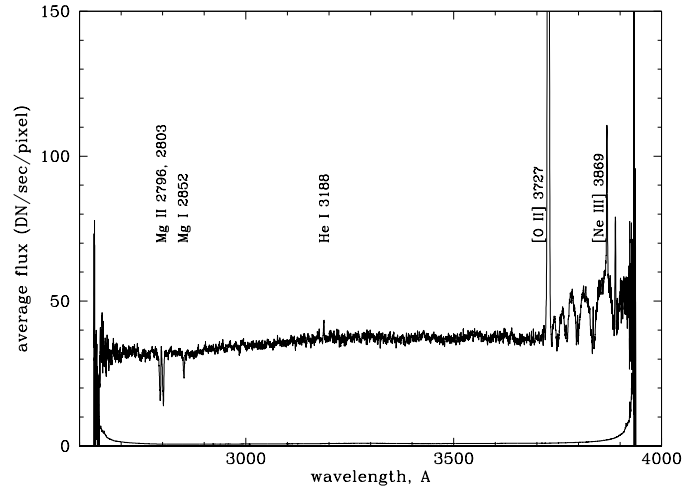


FIG. 2.— The coadded spectrum of all 1406 galaxies in the Mg II sample, in the rest frame. The upper line is the spectrum, smoothed with a 5 pixel boxcar, and the lower smooth line is the error spectrum of the smoothed coadd.

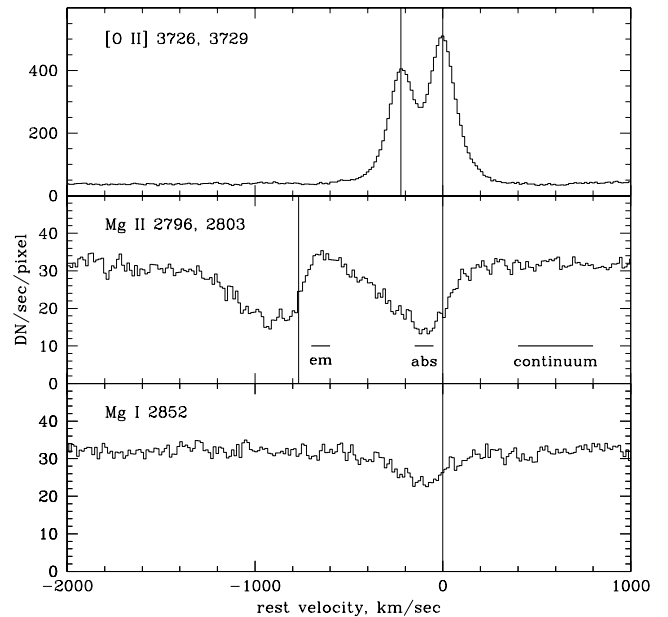


FIG. 3.— The [O II] 3726.0, 3728.8, Mg II 2795.5, 2802.7, and Mg I 2852.1 \AA lines in the coadded spectrum of 1406 galaxies, relative to zero velocity as defined by the redshift derived from [O II]. The [O II] doublet lines are at their nominal systemic velocities, but the Mg I and both Mg II lines show blueshifted and asymmetric absorption profiles. The horizontal bars in the middle panel show the extent of the windows used in Section 3.4 to measure absorption and excess emission in individual spectra.

could be due to wings in individual galaxies or simply the fact that the summation of Gaussians of different dispersions is not itself a Gaussian. In local superwind galaxies, faint optical emission is seen from high-velocity wings of a few hundred km s^{-1} , from shocked gas swept up by the wind (e.g. Bland & Tully 1988; Heckman et al. 1990). The [Ne III] line, which arises in AGN and in very blue starforming galaxies,

is much weaker than [O II], and has a small blueshift of 40 km s⁻¹.

In local luminous infrared and starburst galaxies, the centroid of optical emission can be slightly blueshifted with respect to the systemic velocity, presumably due to emission from outflowing gas. For IR-luminous galaxies, Mirabel & Sanders (1988), found the optical catalog redshift was blueshifted by 90 km s⁻¹ on average relative to the centroid of 21 cm H I emission. In local edge-on starbursts, Lehnert & Heckman (1996) found the nuclear emission lines blueshifted by a median of 25 km s⁻¹ relative to the overall rotation curve. However, in our spectra, since the galaxies are comparable in size to the slit width, [O II] emission is integrated over most of the galaxy. In our coadded spectrum, the velocity of [O II] and the high order Balmer lines at 3798, 3835, and 3889 Å agree well. However, centroiding the broad Balmer stellar absorption lines is difficult due to narrow Balmer emission. We coadded spectra of all DEEP2 blue galaxies at 1.1 < z < 1.5 to reach the Ca II 3933.7 stellar absorption line, and found a negligible offset of < 5 km s⁻¹ between Ca II and [O II].¹² Thus the [O II]-derived redshift is a reliable measure of the systemic velocity.

The Mg II absorption profiles in the middle panel of Figure 3 are strikingly offset from the systemic velocity. Both lines of the Mg II doublet show an asymmetric, blueshifted absorption trough. There is a small amount of absorption redward of systemic to +100 km s⁻¹, a deep trough reaching ~ 60% absorption at a blueshift of -100 km s⁻¹, and an asymmetric, triangular “sawtooth” absorption profile extending blueward beyond -500 km s⁻¹. The Mg I line shows a similar profile, although the depth of absorption is weaker. In the coadded spectrum of the 1406-galaxy sample, the equivalent width of Mg II 2796+2803 absorption is 4.6 Å, and of Mg I 2853 absorption is 0.9 Å.

Between the two Mg II lines, there is a hint that the spectrum goes higher than continuum, at ~ -600 km s⁻¹, or ~ +170 km s⁻¹ relative to the Mg II 2796 line. We study this signature in more detail in Section 3.5, where it is shown to be strong in a small fraction of the sample and due to Mg II emission, most probably from narrow-line AGN.

The velocity offset of Mg II is far greater than the uncertainties in the DEEP2 wavelength scale, as discussed in Section 2. Additionally, the velocity spread of the absorption is greater than the velocity width of the galaxy emission lines, and the asymmetric absorption profile could not arise from calibration errors. Both the blueshift and the asymmetric profile are real properties of the sum of UV emission over the 1406 galaxies.

3.2. The cause of blueshifted absorption

The strong blueshifted absorption shown in Figure 3 is the chief observational result of this paper. It indicates the presence of a significant amount of gas in front of and flowing away from the continuum source at several hundred km s⁻¹ in both Mg II and Mg I, which are low-ionization lines that arise in cool gas. Here we discuss the physical interpretation of this outflow.

The DEEP2 z ~ 1.4 galaxies are small in apparent size; in the subset with HST imaging, 95% have $r_{eff} < 0.95''$. They

are observed with a 1'' slit and the seeing smooths over the galaxy light distribution, so that the continuum in the spectra is the integrated light of the galaxy. Because the absorption reaches > 50% depth, the absorbing material must be spread over the galaxy, rather than, for example, being confined to a nucleus that does not dominate the integrated light.

3.2.1. Circumstellar versus galactic-scale absorption

First we ask whether the absorption is galactic-scale or circumstellar. Hot stars often show ionized outflows in high-ionization lines such as C IV, but do not show outflows in low-ionization lines. Stellar Mg II absorption is weak in luminous, hot O and B stars (Lamers et al. 1973; Lamers & Sijbers 1975; Kondo et al. 1975). Strong and sometimes blueshifted absorption is found in A type supergiants (Praderie et al. 1980; Verdugo et al. 1999). The very brightest and rarest late B, A, and F stars can have asymmetric or blueshifted absorption of order -100 km/s, but fainter stars do not (Snow et al. 1994). Outflows in Mg II are sufficiently infrequent that they should not dominate the integrated light of a star-forming stellar population, and the known stellar outflows are lower velocity than observed in the stacked galaxy spectrum.

The firmest evidence that the outflows seen in DEEP2 are galactic-scale rather than circumstellar comes from the similarity of the Mg II and Mg I outflow profiles. Mg I 2852 is absent in hot stars, present in F stars, but is photospheric and does not show signatures of mass loss (Snow et al. 1994). Circumstellar outflows cannot contribute to the outflow signature in Mg I.

Photospheric, non-outflowing Mg II absorption is weak in very blue stars and stronger in cooler stars (e.g. Rodriguez-Merino et al. 2005). Some of the zero or low-velocity Mg II absorption could be stellar, but this cannot account for the high-velocity blueshifted absorption.

3.2.2. Clustering of intervening absorbers

Intervening Mg II absorption line systems seen against QSOs are known to be associated with normal, relatively luminous galaxies, out to impact parameter ~ 50 kpc, and to be clustered similarly to luminous galaxies (e.g. Steidel & Sargent 1992; Steidel et al. 1994; Bouché et al. 2006; Wild et al. 2008). “Strong” Mg II absorbers (EW > 0.3 Å) have average EW of order $W_{2796} \sim 1 \text{ Å}$ and abundance $dN/dz \sim 1$ (Nestor et al. 2005). One could imagine that absorbers that are not directly associated with the source galaxy, but clustered around it, would produce a blueshifted absorption signature, tailing off to more negative velocities. In this picture the absorption velocity would not represent an outflow but simply the location of the clustered absorbers in the Hubble flow.

However, the absorption strength that could plausibly be produced by nearby clustered absorbers is much lower than we observe. There are a variety of ways of estimating this, which rely on the frequency of intervening absorbers dN/dz , their similar clustering to luminous galaxies, and/or that they are associated with luminous galaxies.

For example, consider absorbers clustered around galaxies with $\xi(r) = (r/r_0)^{-\gamma}$, $r_0 = 4h^{-1}$ Mpc comoving, $\gamma = 1.8$, similar to galaxies and to absorbers clustered around QSOs (Steidel et al. 1994; Coil et al. 2004a; Bouché et al. 2006; Wild et al. 2008). At $z=1.4$, r_0 corresponds to $\Delta z = 0.0029$, or 870 km s⁻¹ in our spectrum. Thus absorbers within r_0 could contribute to the observed absorption. From integrating $\xi(r)$, the overdensity within r_0 is $\delta = 10.5$. The expected strength of

¹² Outflows are rarely seen in Ca II H and K lines in DEEP2, due to stronger stellar absorption, lower abundance than Mg, greater depletion onto dust, and a large ionization correction for Ca II. Similar factors make Ca II rare in QSO absorption line systems (Bowen et al. 1991; Wild et al. 2006).

the absorption is roughly $W_{clust} = \delta \Delta z dN/dz < W_{absorber} >$. From the survey of Nestor et al. (2005), the frequency of absorbers with $W_{rest,2796} > 0.3 \text{ \AA}$ at $z = 1.4$ is $dN/dz = 1.22$, and integrating over the equivalent width distribution yields the mean $< W_{absorber} > = 1.07 \text{ \AA}$. The predicted absorption EW from clustering is then $W_{clust} = 0.04 \text{ \AA}$, a factor of ~ 40 fewer than we observe (Table 1). Essentially, the overdensity within r_0 is not enough to overcome the short pathlength within r_0 , since $dN/dz \sim 1$.

Another way of looking at this problem is that strong intervening Mg II absorbers are associated with luminous galaxies or QSO hosts with impact parameters $\sim 50 \text{ kpc}$ (e.g. Steidel et al. 1994; Hennawi et al. 2006; Chen & Tinker 2008) with a high, but not 100%, covering factor. The absorption EW we observe is $\sim 1.5\times$ the mean of strong Mg II absorbers, $< W_{absorber} >$. To produce the absorption we observe by intervening galaxies, every source galaxy would have to have ~ 1.5 interveners, with 100% covering factors, projected at $< 50 \text{ kpc}$ impact parameter and in front by $\lesssim 800 \text{ km s}^{-1}$. This radius and velocity separation is fairly close to the definition of a close pair, but the fraction of galaxies in close pairs in the DEEP2 sample is only 10% (Lin et al. 2004).

3.2.3. Absorption depth and covering factor

Because the Mg II absorption in Figure 3 is deep, 55% absorption at the bottom of the trough, we know that it covers a large fraction of the UV light over the whole sample of galaxies. It may cover $\sim 55\%$ of the stars in all the galaxies, or all the stars in $\sim 55\%$ of the galaxies, or some compromise. This also helps to confirm that it is from a galactic-scale outflow, rather than from circumstellar outflows associated with a particular type of star, or outflows that are local to an active nucleus.

Winds in local starburst disks are more commonly detected in face-on galaxies (Heckman et al. 2000). The frequency of wind detection in Na I absorption suggests that the angular covering fraction C_Ω of their winds, due to the wind opening angle, is about 0.4-0.5 in starbursts and LIRGs, and higher in ULIRGs (Rupke et al. 2005b). For LIRGs and ULIRGs that do have detected winds, Rupke et al. found a clumpiness covering fraction within the wind of $C_f \sim 0.4$. For a coadded sample of galaxies that all have optically thick winds, the absorption depth is $C_\Omega C_f$, which would be ~ 0.2 in the Rupke et al. sample. An absorption trough depth of 55% is thus quite large compared to the local values, suggesting that winds are actually happening in all of the DEEP2 sample galaxies and that the covering fractions are higher than observed locally in Na I.

Additionally, the Mg I outflow line is not as deep as the Mg II outflow, even though Mg I has a higher oscillator strength and Mg II is saturated. The most likely explanation is that Mg I has a lower covering fraction, and presumably traces denser or cooler parts of the outflow.

Although the blueshifted absorption is from interstellar gas, it is possible that some of the zero-velocity absorption is due to stellar photospheric lines. Separating stellar and ISM contributions typically requires modeling the spectra of star-forming populations with a code such as Starburst99 (Leitherer et al. 1999), but we cannot use it to predict the Mg II line profiles because Starburst99 does not produce high resolution spectra at 2800 \AA . Currently, Starburst99, PEGASE (Fioc & Rocca-Volmerange 1997), and the models of Bruzual & Charlot (2003) are all limited to resolutions $\sim 10 \text{ \AA}$ at 2800

\AA , which limits our ability to model the Mg II line profiles or EW expected from given stellar populations. However, we can decompose the absorption into velocity components to separate the outflow and zero-velocity, non-outflowing components (Section 4).

3.2.4. The possibility of AGN-driven outflows

Active galactic nuclei are known to drive winds and sometimes show blueshifted absorption outflow signatures (e.g. Crenshaw et al. 1999; Veilleux et al. 2005; Trump et al. 2006; Wild et al. 2008). AGN outflows in Mg II are seen in low-ionization BAL QSOs, which are a few percent of all QSOs (Trump et al. 2006), and in 1 of 17 Seyfert nuclei studied by Crenshaw et al. (1999). AGN/starburst composite IR-luminous galaxies often show low-ionization outflows traced by Na I (Rupke et al. 2005c). There are signs that the Na I outflows in AGN/starburst composites are different on average from those in starburst IR-luminous galaxies, with lower opening angle and higher velocity. However, the AGN does not dominate the large scale outflow in these galaxies (Rupke et al. 2005c).

The high frequency and covering fraction of absorption in the DEEP2 galaxy sample suggests that the outflows are driven by star formation rather than AGN. Nearly all blue cloud galaxies are star-forming, while luminous AGN are much rarer than 50% and are not common in blue star-forming galaxies at $z \sim 0.8 - 1$, as measured by X-ray or emission line signatures; AGN signatures are more often seen in red or intermediate-color galaxies (Nandra et al. 2007; Weiner et al. 2007). Further, Mg II absorption occurs in just a few percent of AGN, as described above. Some of the galaxies in our sample may have AGN producing Mg II emission, discussed in Section 3.5, but this does not appear to be correlated with the galactic-scale Mg II absorption.

3.3. Absorption detected in individual spectra

We examined the individual spectra in the 1406-galaxy sample at the location of Mg II. Figure 4 shows six illustrative spectra. The top five panels have relatively high S/N; the top three panels show blueshifted Mg II absorption, and panels 4 and 5 show narrow Mg II emission. Many of the spectra do not have a high S/N in the continuum and we neither detect nor rule out Mg II absorption. The lowest panel of Figure 4 shows one such typical spectrum. As discussed in Section 3.4, in the aggregate, these spectra do show Mg II absorption.

About 5-10% of the individual spectra are high enough S/N to show convincing Mg II absorption. When it is seen, it is almost always blueshifted. The top three panels of Figure 4 show examples of blueshifted absorption; the third object has especially strong absorption. Note that the individual galaxies have asymmetric sawtooth absorption profiles just as the coadded spectrum in Figure 3 does - there is a long tail to high velocities. The sawtooth profile is a property of individual winds, not just caused by the coadding process.

About 4% of the individual spectra show fairly narrow Mg II emission lines, as seen in panels 4 and 5 of Figure 4. This is not characteristic of star formation and probably comes from Seyfert nuclei or other narrow-line AGN. The Mg II emission is generally at the systemic velocity. The emission is sometimes accompanied by detectable blueshifted absorption, but less than 50% of emission objects have individually detectable absorption. In Section 3.5 we discuss the properties of these excess-emission objects.

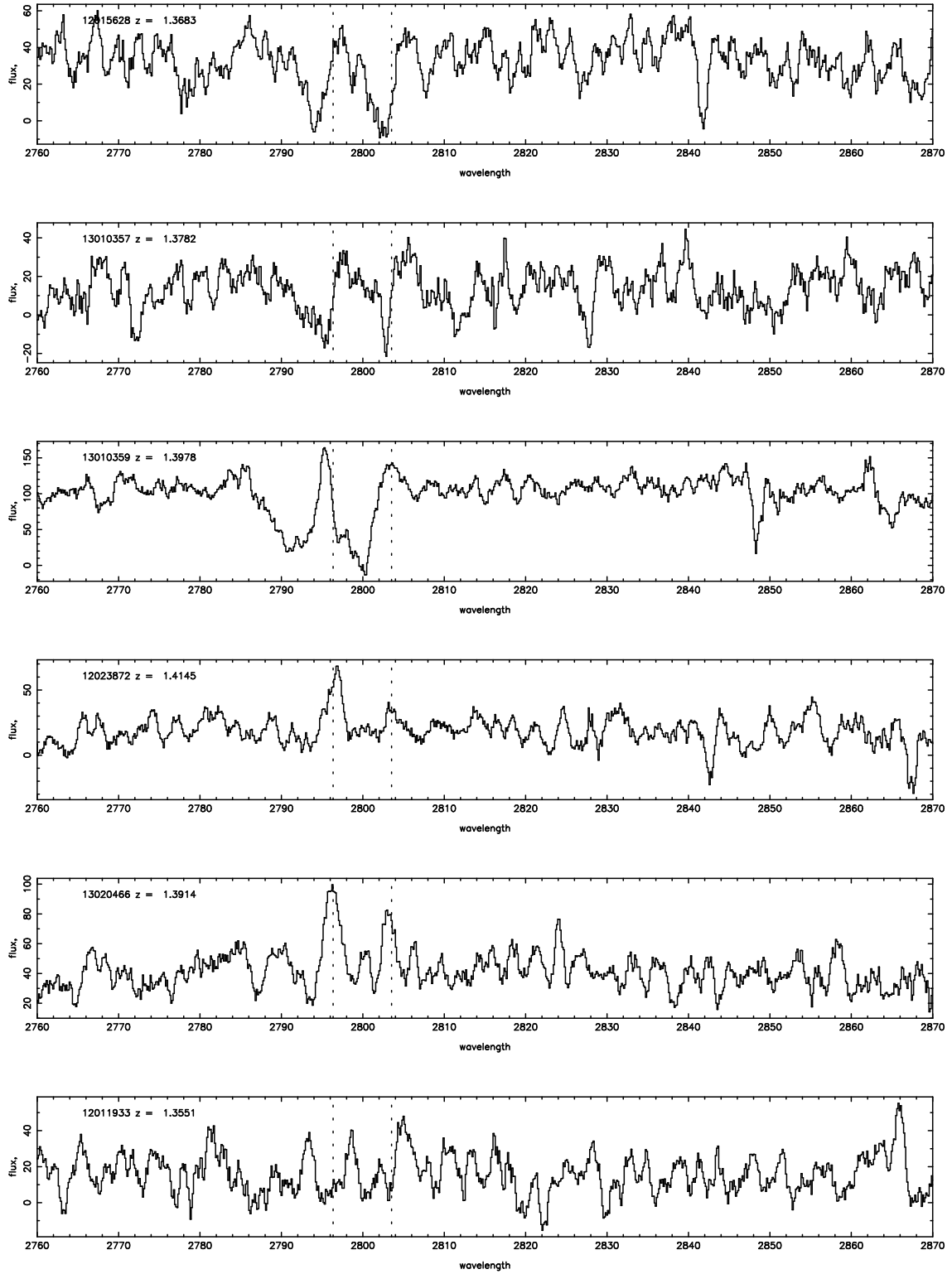


FIG. 4.— DEIMOS spectra of six galaxies in the Mg II sample in the rest frame. The spectra have been smoothed by a 9 pixel boxcar (1.25 \AA in the rest frame). Vertical dotted lines indicate the systemic velocity of Mg II $\lambda\lambda$ 2796, 2803. The top three illustrate the $\sim 5 - 10\%$ of the sample that clearly show blueshifted absorption in individual spectra, with a broad asymmetric profile. Spectra 4 and 5 show narrow Mg II emission at the systemic velocity, visible in $\sim 5\%$ of the spectra, presumably due to narrow-line AGN. The spectrum in the bottom panel is more typical of the majority of the sample, where Mg II is neither individually detected nor ruled out. The units of the spectra are e-/hour and the typical noise is 40-50 e-/hour/pixel before smoothing.

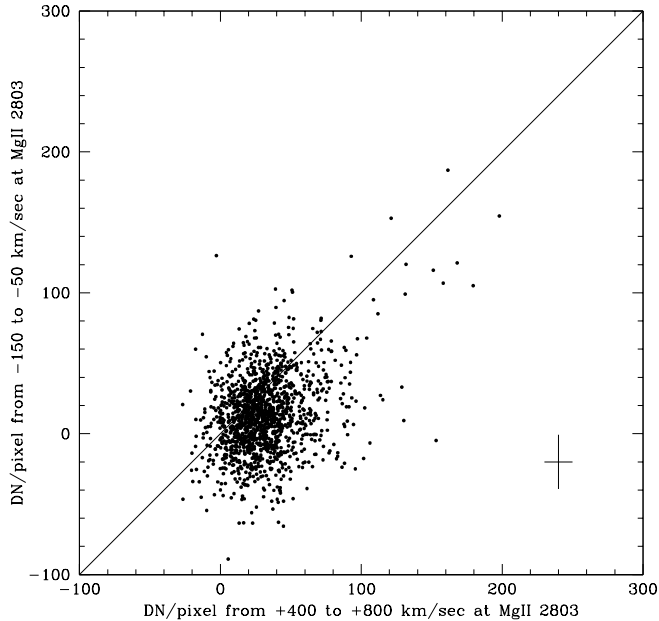


FIG. 5.— Flux decrement blueward of Mg II 2803 in individual galaxies. The error cross shows the median error bar. The whole distribution is shifted, with the flux density at -150 to -50 km s^{-1} systematically below the continuum.

3.4. Flux decrements in individual galaxies

In any coadded spectrum or stacked image detection, one has to ask if a feature is a general property of the sample or is caused by a small fraction of outlier objects, and if the feature is weighted more or less to brighter objects. This is a less severe problem for absorption than for emission lines, but is still of interest.

Each individual DEEP2 galaxy spectrum has low S/N/pixel at 2800 \AA . To address the effect of stacking, for each spectrum we compute the average pixel value and its error estimate in three windows relative to the Mg II 2802.7 line: (1) $+400$ to $+800 \text{ km s}^{-1}$, (2) -150 to -50 km s^{-1} , and (3) -700 to -600 km s^{-1} . Window 1 measures the continuum level, window 2 is located at the deepest part of the blueshifted Mg II 2802.7 absorption, and window 3 is at the high point between the two Mg II lines, where there may be excess emission above continuum. The locations of these windows are shown in the middle panel of Figure 3.

Figure 5 compares the average flux in the continuum window 1 and the absorption window 2. There is considerable scatter, as expected given the median errorbar, but the entire distribution of points is shifted below the 1:1 line. The blueshifted absorption is a phenomenon that occurs throughout the $z = 1.4$ galaxy sample, not in just a small subset.

Figure 6 compares the average flux in the continuum window 1 and the excess emission window 3, between the Mg II absorption lines. The behavior here is rather different than in Figure 5. The bulk of galaxies scatter around the 1:1 line; they are roughly at the continuum level in window 3. However, a small number of galaxies show significant excess emission in window 3. These are relatively bright and so contribute to the light-weighted coadded spectrum. We discuss these unusual objects in the next section.

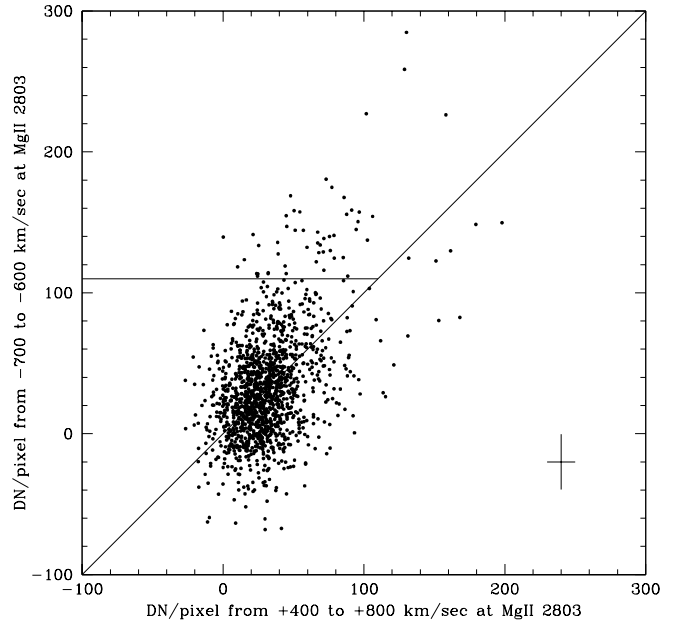


FIG. 6.— Flux increment between the two Mg II absorption lines in individual galaxies. A tail of objects have enhanced emission above continuum in the window at -700 to -600 km s^{-1} relative to Mg II 2802.7, or $+69$ to $+169$ relative to Mg II 2795.5 \AA . The error cross shows the median error bar. The horizontal line at 110 DN/pixel defines the “excess emission” galaxies.

3.5. Galaxies with excess Mg II emission

We define the “excess emission sample” as the tail of 50 objects with $\text{flux}(\text{window } 3) > 110 \text{ DN/pixel}$ and $\text{flux}(\text{window } 3) > \text{flux}(\text{window } 1)$. These galaxies tend to be in the bluer half of the sample and brighter than average, as shown in the magnitude-color diagram of Figure 7.

Figure 8 shows the coadded spectra of the 1356 galaxies without excess emission and the 50 galaxies with it (lower panel). When these 50 galaxies are coadded, they show a clear signature of emission around $+100 \text{ km s}^{-1}$ relative to 2795.5 \AA and at $+100 \text{ km s}^{-1}$ relative to 2802.7 \AA . In the “no-excess emission” sample (middle panel of Figure 8), the spectrum as observed does not have an excess above continuum, but modeling the red wings of the two Mg II lines suggests a small excess, discussed further in Section 4.

On examining the individual spectra in the excess-emission galaxies, a number of them show relatively weak Mg II emission lines with FWHM ~ 150 to 300 km s^{-1} , in which the doublet is resolved. This Mg II emission is weaker and narrower than the broad Mg II of QSOs, and is probably from Seyfert nuclei (e.g. Wu, Boggess & Gull 1983). Another possibility is redshifted emission from the back side of the wind; this has been observed locally in the Na I line in the galactic wind of NGC 1808 (Phillips 1993). Chromospheric Mg II emission from stars is unlikely to be the cause, especially since it is less strong in hot stars (e.g. Snow et al. 1994), and the emission we see is stronger in bluer galaxies.

Some of the excess-emission spectra also show Mg II absorption, near systemic velocity or blueshifted by a few hundred km s^{-1} . At first glance the composite spectrum in the lower panel of Figure 8 resembles the redshifted emission in P Cygni absorption/emission profiles, but the emission in individual spectra is generally near the systemic velocity. Many

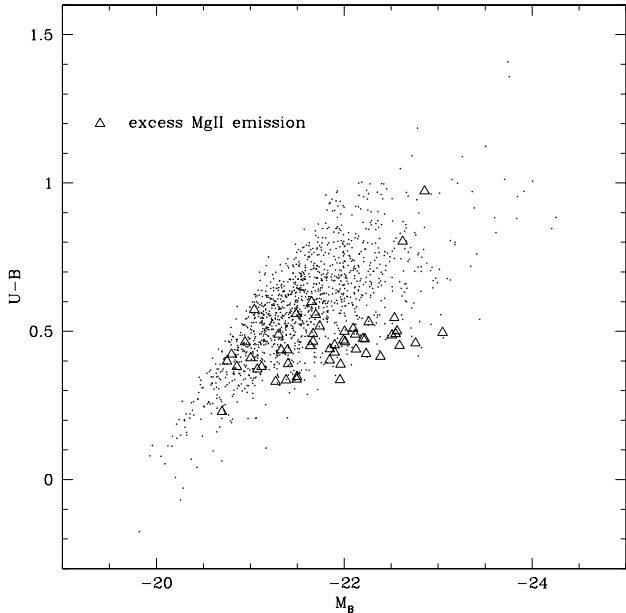


FIG. 7.— The magnitude-color distribution of the Mg II 1496-galaxy sample in restframe M_B and $U - B$. Galaxies with excess Mg II emission above continuum are plotted as large open triangles. The emission is likely from narrow-line AGN and the objects are among the brighter of blue galaxies.

objects in the excess-emission sample do not have a P Cygni profile, but in the coadded spectrum, the overall blueshifted absorption eats away at the Seyfert emission lines.

In the lower panel of Figure 8, the emission peak of the Mg II 2795.5 line is higher, and the continuum is not flat, showing “shoulders” out to $\sim 600 \text{ km s}^{-1}$ away from the Mg II lines. The bluer Mg II line has a higher g -factor and should be stronger. More exotically, it is also possible that the line contains some weak broad Mg II AGN emission, which is then partially absorbed by blueshifted gas, leaving a trace of asymmetry and the broad continuum shoulders. We searched for Ne V AGN emission at 3425 \AA but did not detect any in coadds of either the excess or no-excess spectra.

If the Mg II emission is from AGN, it is not clear why it is strongest in the bluest and lower-mass subsample. Some AGN light might be contributing to the galaxy color and luminosity. The emission might also be redshifted from the far, receding side of the wind, as in P Cygni profiles. Blueshifted absorption and redshifted emission is seen in the Na I D line in the wind of the star-forming galaxy NGC 1808 (Phillips 1993), where the wind is found across the disk and is due to star formation rather than nuclear activity. However, it is not clear why back side emission would be stronger in the bluer galaxies. Bluer, lower-mass galaxies might have less internal extinction so that it is easier to see the back side of the wind. But this does not appear to explain the individual Mg II lines that are at the systemic velocity. Interpretations of the emission are hampered by the lack of moderate-resolution Mg II spectra in local galaxies to use as a comparison.

The excess-emission sample appears to contain relatively faint narrow-line AGN, some detected in individual spectra in Mg II emission, and possibly low-level broad-line AGN, or back-side wind emission. However, the strength of blueshifted absorption is similar between the composite of this

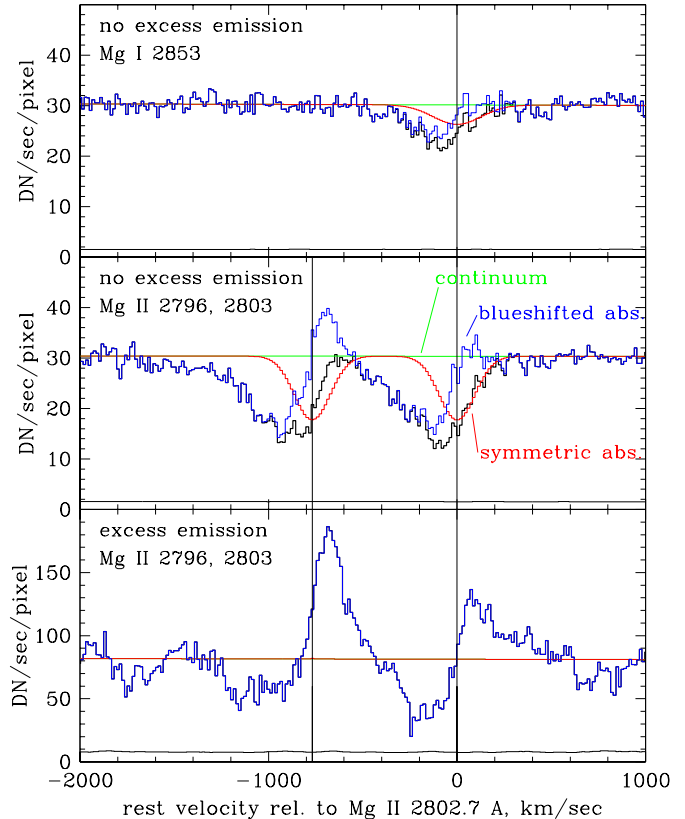


FIG. 8.— Absorption profiles for: Mg I 2852 \AA for 1356 galaxies without excess Mg II emission (upper panel); Mg II $2796, 2803 \text{ \AA}$ for the same 1356 galaxies (middle panel); and 50 galaxies with excess Mg II emission between the two absorption lines (lower panel). The colored lines in the middle and upper panels show decompositions into continuum (green straight line), symmetric absorption (red gaussians) and outflow absorption (blue), discussed below in Section 4. The horizontal black line near zero is the error array for the coadded spectrum.

sample and of the remaining 1356 galaxies: the outflow component seems to be independent of the presence of the AGN.

Because the excess-emission galaxies have a distinctly different spectral shape and the underlying emission makes it harder to measure the properties of the absorption, we exclude them from the discussion of Section 6 where we measure the dependence of the absorption on galaxy properties. When the remaining 1356 galaxies are analyzed, we do see some residual emission, especially in the bluer galaxies; see Section 4.

4. INTRINSIC AND OUTFLOW ABSORPTION

The spectra shown in Figure 3 show Mg I and Mg II absorption that is asymmetric but with both blue and red-shifted absorption. We propose a simple model to decompose the absorption into two physically meaningful components: intrinsic and outflow.

4.1. Decomposition into symmetric and blueshifted absorption

In composite spectra, we cannot hope to resolve individual absorption systems. We aim to differentiate intrinsic absorption within the galaxy at the systemic velocity from outflow absorption at negative velocities. The task is complicated by

the fact that Mg II is a doublet. Our approach is to measure the absorption at systemic velocities from the red side of the redder Mg II line and the outflow in the blue side of the bluer line. A main goal of this decomposition is to avoid counting intrinsic absorption in the wind opacity; the results on outflows are not very sensitive to the details of the method.

Suppose that a spectrum is produced by a galaxy with a mix of UV-emitting stars and gas with some velocity dispersion or rotation, and surrounded by a wind of outflowing material. The actual line-of-sight velocity of the galactic ISM absorption will depend on the geometry of the galaxy, but when a large number of spectra are coadded, this should average out, so that absorption due to galactic gas will have roughly zero mean velocity and the average velocity spread of the coadded galaxies. Stellar photospheric absorption will have a zero mean velocity and width governed by the stellar atmospheres. The intrinsic ISM+stars component should be symmetric about zero velocity, and its red wing can produce the positive-velocity absorption.

In principle, inflow of gas accreting onto the galaxy could also contribute to the red wing. However, infalling gas whose kinematics are governed by gravitation will be at velocities of order the virial velocity dispersion of the halo, and it is very difficult, even if gas is detected, to separate inflow from any other gas associated with the galaxy. In contrast, outflowing gas with kinematics set by star formation or AGN can be distinguished.

Outflowing gas that lies between the UV source and us will absorb at blueshifted, negative velocities. This gas could have some velocity dispersion, but it should be fairly small in cool gas (e.g. Rupke et al. 2005a). To determine properties of the outflowing component, we attempt to separate it from the intrinsic component. We adopt the model:

$$F_{obs}(\lambda) = CF_{em}(1 - A_{sym})(1 - A_{flow}), \quad (1)$$

$$A_{sym}(\lambda) = A_1 G(v, \lambda_1, \sigma) + A_2 G(v, \lambda_2, \sigma) \quad (2)$$

where $F_{obs}(\lambda)$ is the observed flux density, $C(\lambda)$ is the underlying linear fit to the continuum of the galaxy, $F_{em}(\lambda)$ describes any variation in the emission beyond the linear continuum slope, and A_{sym} and A_{flow} are the depths of the intrinsic (symmetric) and outflow (blueshifted) absorption. We model the symmetric absorption as the product of two Gaussians $G(v)$ centered on the wavelengths λ_1, λ_2 of the two Mg II lines, with velocity dispersion σ and intensities A_1, A_2 .

The result of this model is illustrated in the middle panel of Figure 8. The heavy black line is the observed spectrum; the green straight line is the continuum fit, the red double Gaussian absorption lines are the symmetric component $A_{sym} = A_1 G(2796) + A_2 G(2803)$, and the blue line is the outflow component $1 - A_{flow}$ that remains after the observed spectrum is multiplied back by $1 - A_{sym}$.

The relative intensities of the absorption in the two lines depend on the balance between optical depth and covering factor.¹³ For the Mg II doublet, the g -value of the bluer line and its oscillator strength are twice as large, so in optically thin absorption the bluer line is twice as strong, while in optically thick absorption the strengths are equal. The Mg II

transition becomes optically thick at a low column density ($N_{MgII} \gtrsim 10^{13}$ atoms cm^{-2} , or $N_H > 10^{18}$ for solar abundance), so it is generally saturated in cool gas and in stars. In our spectra the depths of the Mg II lines appear equal, so we set $A_1 = A_2$, implying saturated absorption in the symmetric component.

Decomposing the symmetric and blueshifted components can be awkward due to the doublet. We infer the properties of the symmetric components from the red side of the red line. By assuming symmetry, we can determine how much of the absorption at negative velocities is actually due to the symmetric component. We assume the strengths of the two Mg II lines are equal to infer the symmetric component of the bluer line.

The upper two panels of Figure 8 illustrate the decomposition applied to the Mg II and Mg I 2852 lines. The x-axis is velocity referenced to the $\lambda = 2802.7$ or the $\lambda = 2852.1$ line. We first fit the linear continuum $C(v)$ by averaging the data in two windows at $-2400 < v < -1600$ km s^{-1} and $800 < v < 1600$ km s^{-1} , and interpolating between those points. We divide the observed spectrum by the continuum so that the line strengths are fitted to a spectrum normalized to 1.

We then fit a Gaussian line profile $A_2 G(v, \lambda_0 = 2802.71, \sigma)$ to the positive velocity data of $1 - F_{obs}/C$, using only the pixels at $0 < v < 1600$ km s^{-1} . The fitted parameters are a constant continuum level, the intensity A_2 , and the dispersion σ ; the central velocity is held fixed at 0. The parameters are tabulated in Table 1. The dispersion is due to both velocity dispersion and the intrinsic widths of stellar Mg II lines, which can be large for cooler stars. The fit is performed using a Levenberg-Marquardt non-linear least squares minimization. Setting $A_1 = A_2$, we duplicate this Gaussian for the bluer Mg II line to make $A_{sym}(v)$.

Knowing $F_{obs}(v)$, $C(v)$, and $A_{sym}(v)$, we obtain $F_{em}(v) \times (1 - A_{flow}(v))$. If the galaxy emission is featureless, then $F_{em} = 1$ and we have measured the absorption of the outflow component A_{flow} . If there is some residual Mg II emission, then $F_{em}(v)$ can be > 1 and we may underestimate the depth of the outflow absorption. This is a fairly small effect once the 50 excess-emission galaxies have been removed from the sample, but reappears in the subsample of the bluest galaxies (Section 6).

Ultimately, the details of decomposing the symmetric absorption do not have a strong effect on the interpretation of the wind component. We attempt this decomposition to keep from erroneously counting too much symmetric absorption in the wind; this is important since some of the symmetric absorption in both Mg II and Mg I could be due to photospheric or zero-velocity ISM rather than outflow absorption, especially in galaxies with many cool stars. There are some degeneracies between the fit parameters, e.g. the allocation of absorption EW between symmetric and blueshifted components; the approach is only robust when the composite spectra are high S/N to constrain the symmetric component, which is fit to one side of a Gaussian. These issues do not affect our conclusions; we do find that both the symmetric and the wind components have the same dependence on galaxy properties – they are stronger in more massive objects, as we show below.

The middle and upper panels of Figure 8 show the coadded spectrum F_{obs} of the 1356 galaxies excluding the excess emission sample, the symmetric Mg II doublet absorption (multiplied back by the continuum), $C(1 - A_{sym})$, and the outflow component (also multiplied by C), $C(1 - A_{flow})F_{em}$. Proper-

¹³ For individual absorption systems, one must also consider the possibility that spectrograph resolution dilutes unresolved but saturated lines. Our measurements are of an ensemble of coadded absorbers, and the ensemble is resolved though individual clouds are not.

ties including EW and velocities of the components are tabulated in Table 1.

4.2. Optical thickness of the absorption

In optically thin Mg II absorption, the 2796 Å line is twice as strong as the 2803 Å line. However, Mg II absorbers are frequently optically thick and saturated, in which case the line depths are close to equal (e.g. Steidel & Sargent 1992).

The symmetric Gaussian model goes deeper than the red wing of the 2796 Å absorption, which causes the inferred outflow $F_{em}(1 - A_{flow})$ (blue line in middle panel of Figure 8) to still show some excess emission, even though the strong excess-emission galaxies have been weeded out. The cause must be excess emission, since the 2796 Å symmetric line cannot be intrinsically weaker than the 2803 Å line.

In the spectrum of Figure 8 (middle panel), the EWs of the outflow absorption component from 0 to -768 km s^{-1} are 1.54 and 1.37 Å for the 2796 and 2803 Å lines, (excluding pixels above continuum to avoid diluting the blueshifted 2803 Å line by emission in the 2796 Å line). This yields a doublet ratio of 1.13, implying quite saturated absorption. Even this is an upper limit since the 2803 blueshifted absorption depth is still reduced by some emission in the 2796 line. The absorption troughs reach equal depths at -100 km s^{-1} relative to each line, suggesting that the true line ratio is close to 1.0 and the Mg II is highly saturated. We discuss the depth and column density further in Section 7.1. For saturated absorption, the equivalent width is more directly controlled by the velocity spread than the column density.

The Mg II absorption in both the symmetric and outflow components is not optically thin, so a distribution of column density $N_H(v)$ that is Gaussian in velocity can not produce an optical depth or absorption $A(v)$ that is Gaussian. For a more detailed discussion of the interaction of optical depth and covering fraction, see Rupke et al. (2005a). However, a superposition of a Gaussian velocity distribution of small velocity-width clouds, each of which is optically thick but has a small covering fraction, can produce a Gaussian line. Stellar photospheric profiles can also be fit by a Gaussian.

In practice, the coadded spectra and blended doublet do not allow us to separate optical depth and covering fraction. A Gaussian is a reasonable fit to the red wing, while for the blueshifted absorption, the coaddition of many spectra is analogous to an ensemble of absorbers over a range of optical depth and velocity spread, as modeled by Jenkins (1986) in testing the applicability of the classical doublet ratio method (Spitzer 1986). We use the ratio of the two Mg II lines to estimate the optical depth and column density in Section 7.1.

As Figure 8 shows, the Mg II absorption trough can extend quite far to the blue, well beyond -600 km s^{-1} relative to the 2796 Å line. It is difficult to measure the extent of blueshifted absorption in the 2803 Å line because it runs into the 2796 Å line and excess emission. In the deepest part of the absorption trough, the two lines agree well. If the lines become optically thin at high negative velocities, the 2796 Å line would be stronger, but this is difficult to measure given blending and a possibly non-flat continuum. The Mg I 2852 Å line is weaker than the Mg II lines but has a similar velocity profile and ratio of blueshifted to symmetric absorption.

4.3. The sawtooth outflow profile

The velocity profile of the Mg II blueshifted absorption in the coadded spectrum shows a characteristic asymmetric or “sawtooth” shape, with its deepest point around -150 km s^{-1} and lower absorption at large negative velocities out to nearly -1000 km s^{-1} . The Mg I profile has a similar shape. This sawtooth shape also appears when the sample is subdivided based on galaxy properties such as mass and star formation rate (Section 6). The asymmetric line shape is also seen in absorption in individual galaxy spectra, as shown in Figure 4. Some individual galaxies could have narrower, distinct absorption systems, as seen in high-resolution spectroscopy of low-redshift outflows (Schwartz & Martin 2004; Rupke & Veilleux 2005; see also the simulations of Fujita et al. 2008).

In our coadded spectrum, the sawtooth profile expresses the mean absorption in front of star-forming galaxies as a function of velocity. Individual absorbers are probably optically thick, but the covering factor is less than 100%, so the mean absorption depth is essentially the probability of finding a absorber at that velocity. Because individual galaxies exhibit the asymmetric absorption profile (at least in galaxies bright enough to see absorption individually), it seems to be a property of the wind physics rather than of the distribution of wind velocities over the ensemble. This appears to rule out two toy models for the sawtooth profile: (1) it is solely due to a distribution of characteristic wind velocities that has fewer winds at high velocity; (2) the winds are well-collimated, and the profile arises as we stack fewer galaxies with high outflow velocities because face-on galaxies are rarer. We discuss an interpretation of the sawtooth profile in terms of cool gas being accelerated by the wind in Section 7.4.

5. PROPERTIES OF THE SAMPLE GALAXIES

The large number of galaxies in the Mg II sample allows us to measure the dependence of outflows on host galaxy properties by dividing the sample into several parts and coadding them separately. We compute restframe magnitude and color, and stellar mass and star formation rate. In this section, we describe how these are computed from the *BRI* magnitudes and spectra, the calibration to stellar masses from *K* magnitudes, and calibration of UV SFRs to MIPS $24\mu\text{m}$ fluxes. Because the Mg II sample is selected at restframe 2800 Å, there are strong covariances among some of the properties such as mass and star formation rate. The distribution of the sample in several properties is shown in Figures 10 and 12.

5.1. Magnitudes and colors

To derive rest magnitudes, we use an SED interpolation procedure, previously described and tested in Weiner et al. (2005) and Willmer et al. (2006). For a DEEP2 galaxy at some redshift z , we redshift the UV+optical SEDs of 34 actual galaxies from the atlas of Kinney et al. (1996), compute the desired restframe quantity, e.g. restframe $U - B$ color, as a function of an observed color, e.g. $R - I$, and combine the relation derived from the SEDs with the actual $R - I$ color of the DEEP2 galaxy to infer its restframe $U - B$ color. At $z \sim 1.4$, the DEEP2 *BRI* filters correspond roughly to restframe 1800 Å, 2800 Å, and *U*-band. Inferring a blue magnitude M_B and $U - B$ color effectively extrapolates from a 2800 – *U* observation, so the zeropoint of our $U - B$ color scale might suffer shifts of 0.1 – 0.2 magnitudes when compared to lower redshift data. However, relative measurements of color within our sample are accurate. The UV magnitudes M_{2800} and M_U are measured quite accurately by our procedure

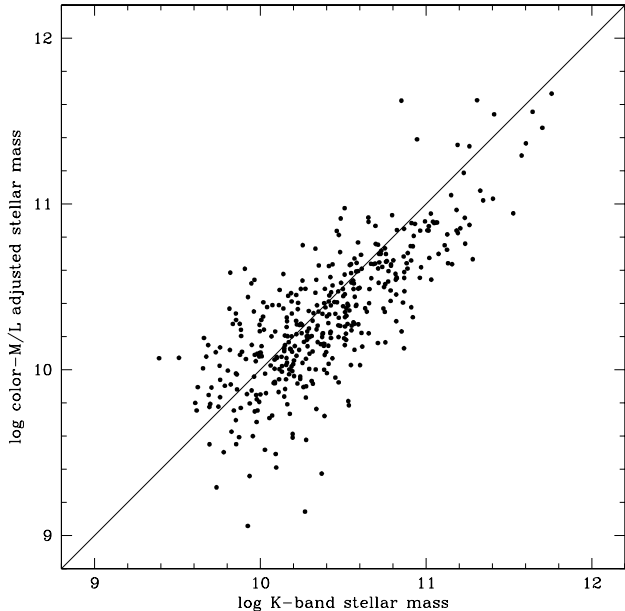


FIG. 9.— Stellar mass estimates from the SED fitting of Bundy et al. (2006) including the K -band (x-axis) and from the optical color- M/L relation empirically corrected to K -band masses (y-axis). There is an offset of 0.09 dex and RMS dispersion of 0.3 dex, but good overall agreement.

since they correspond closely to the observed RI filters. We also estimate UV magnitudes at 1500 and 2200 Å, close to the GALEX FUV and NUV bandpasses.

5.2. Stellar masses

Stellar masses are best derived from the infrared, but near-IR photometry does not exist for our entire sample. For 33% of galaxies with redshifts in the DEEP2 survey, K magnitudes and stellar masses were measured with the Palomar 5-m telescope and WIRC camera, over ~ 80 nights of imaging (Bundy et al. 2006; Conselice et al. 2008). The remaining two-thirds do not have K magnitudes because the Palomar/WIRC survey does not cover all of the DEEP2 area and misses some fainter galaxies in regions where it is less deep. We use the rest M_B and $U - B$ to derive a stellar mass (M_*) estimate using color- M/L relations (Bell & de Jong 2001; Bell et al. 2003) and then empirically correct these to stellar masses computed using K -band photometry and SED fitting by Bundy et al. (2006). This is a revision of a similar calibration computed in Lin et al. (2007). The details of the calibration and formulae which can be used to derive M_* for DEEP2 galaxies are given in Appendix A.

Figure 9 compares the resulting mass estimates from color- M/L to those from K -band; both are for a Chabrier IMF. The color- M/L masses are 0.09 dex lower with an RMS dispersion of 0.30 dex. Although there may be remaining systematics, the relative order of M_* is reliable; our sample spans ~ 1.5 dex in stellar mass, containing both low-mass blue galaxies and higher-mass intermediate-color galaxies. The agreement in mass estimate allows using the color- M/L relation uniformly over the sample, since K is not always available. Figure 10 compares color, magnitude and stellar mass for the sample.

5.3. Emission line luminosities and velocities

The primary emission line found in the Mg II sample is the [O II] 3727 Å doublet. We measure its intensity and width as described briefly in Weiner et al. (2007): in each DEEP2 1-d extracted spectrum, we perform a non-linear least squares fit of a double Gaussian, with the doublet line separation fixed but the intensity ratio allowed to vary (although it is generally consistent with the mean value of 1.4). Each fit yields a measurement of the intensity of the doublet, its location, and the velocity dispersion. A similar procedure is used to measure the velocity dispersion in the stacked spectra.

We compute a line equivalent width from the intensity and a continuum measured over a 90 Å window. The EW and the calibrated BRI photometry are combined to obtain a total rest-frame line luminosity. This procedure bypasses instrumental throughput, and calibrates out slit losses as long as the ratio of emission to continuum is the same inside the slit and outside. For high- z DEEP2 galaxies, which nearly always have $r_{eff} < 1''$, the small size and seeing make this a safe assumption.

The typical [O II] luminosity is high, $\sim 10^{42}$ erg s $^{-1}$, and $L([\text{O II}])$ increases with M_B or mass, as does the UV SFR estimate described below. However, we found that deriving star formation rates from [O II] luminosity is quite dependent on assumptions about the metallicity and extinction (e.g. Kewley et al. 2004; Weiner et al. 2007). These are unmeasured for this sample, and we expect evolution in them compared to lower-redshift samples (Shapley et al. 2005). Locally and at $z \sim 0.8$, there are also strong trends in nebular line ratios as a function of mass (Moustakas, Kennicutt & Tremonti 2006; Weiner et al. 2007). Without a calibration of these trends, SFR estimates from [O II] can be systematically off. Applying a low-redshift calibration (e.g. from Kennicutt 1998) produces SFRs that are ~ 0.5 dex above the IR and far-UV SFR indicators discussed in the next section. We advise caution in applying [O II] SFRs at $z > 1$ without better calibrations, which are beyond the scope of this paper.

5.4. Star formation rates

Estimating star formation rates for high- z galaxies generally relies on local calibrations and models. No SFR estimators at high redshift are both sensitive and well tested; emission-line and UV estimators are affected by extinction, while mid-IR surveys detect fewer objects and may be affected by uncertainties in the IR SEDs. We explore both IR and far-UV estimates of the SFR, keeping in mind that there may be systematic effects. In the end we are able to reconcile these estimates by stacking the far-IR data.

5.4.1. SFR from mid-infrared luminosity

The mid- to far-IR luminosity emitted by dust heated by young stars yields an estimate of the SFR that is not affected by extinction, though it can be affected by AGN emission and by variations in the IR SEDs. Although only a small number of galaxies are detected in the IR, the SFR(IR) is valuable both for calibrating UV and optical estimates of SFR, and for comparing to studies of outflows in local IR-luminous galaxies (Heckman et al. 2000; Rupke et al. 2005a; Martin 2005).

One DEEP2 field, the Extended Groth Strip, has been imaged at 24 μm by scan mapping with MIPS, the Multiband Imaging Photometer for Spitzer (Rieke et al. 2004), to a sensitivity of 83 μJy at $\sim 5\sigma$. We matched the DEEP2 galaxies to a catalog of 24 μm fluxes constructed by PSF fitting (Davis et al. 2007). Of the 1406-galaxy sample, 194 are in the area imaged by MIPS at 24 μm and 38 galaxies are detected.

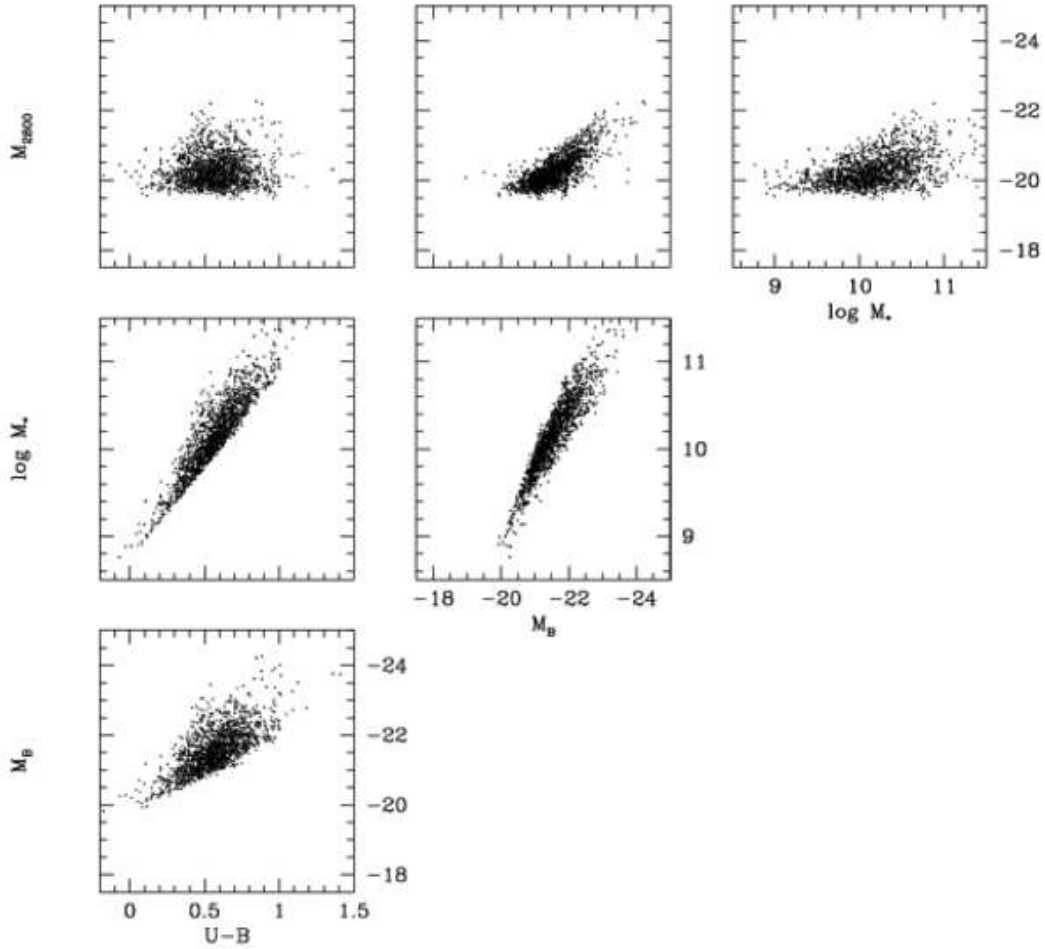


FIG. 10.— Magnitude, color, and stellar mass estimates for galaxies in the Mg II sample. The axes span 7.5 mag or 3 dex for magnitude and mass. The dependence of stellar mass on color means that the sample spans a wider range of mass than UV or blue magnitude.

We estimate a total infrared luminosity $L_{IR}(8 - 1000\mu\text{m})$ from the $24\mu\text{m}$ flux using an SED of Dale & Helou (2002) with $\alpha = 2.0$, which is applicable to star-forming galaxies and follows the average trend of $8 - 24\mu\text{m}$ color with redshift in DEEP2 galaxies. Using this SED produces K-corrections similar to those obtained by averaging a large number of Dale & Helou SEDs, as done by Bell et al. (2005). At $z = 1.4$, the conversion is not a strong function of redshift, and $\log L_{IR}(L_{\odot}) \simeq \log S_{24} + 9.63$, with S_{24} in μJy . The $83\mu\text{Jy}$ limit corresponds to an IR luminosity of $10^{11.5} L_{\odot}$, and the median $\log L_{IR}$ is 11.73. 34 of the 38 MIPS-detected sources are luminous infrared galaxies (LIRGs, $L_{IR} > 10^{11} L_{\odot}$), and four of the 38 galaxies have $L_{IR} > 10^{12} L_{\odot}$, and are ultraluminous infrared galaxies (ULIRGs).

We estimate star formation rates by combining the UV(2800 Å) and IR luminosities, using the prescription of Bell et al. (2005):

$$SFR(IR) = 9.8 \times 10^{-11} (L_{IR} + 2.2\nu L(2800\text{ Å})) \quad (3)$$

where L_{IR} and $L(2800) = 1.5\nu I_{\nu}(2800\text{ Å})$ are in solar luminosities; this is defined for a Kroupa IMF (Kroupa 2001). The

IR term dominates this sum; in the MIPS-detected sample, the median $\log L_{IR}/(2.2\nu L(2800))$ is 0.9 dex.

Because the MIPS galaxies are IR-selected, they will have a larger IR/UV than typical. It is also possible that AGN contribute to the IR luminosity in some of the objects. However, only one of the 38 MIPS sources is also among the 50 excess Mg II emission AGN objects. Another systematic effect is the use of a single typical star-forming IR SED to convert to total L_{IR} . At $z = 1.4$ the $24\mu\text{m}$ band of MIPS is at rest-frame $10\mu\text{m}$, and the observed flux could be enhanced by PAH emission or depressed by silicate absorption. Additionally, the dust temperature could be different from local galaxies; Papovich et al. (2007) and Rigby et al. (2008) find that the $24\mu\text{m}$ flux can overestimate the SFR in IR-luminous $z \sim 2$ galaxies. These issues are difficult to calibrate out; they probably contribute of order 0.3 dex scatter to the $SFR(IR)$ (e.g. Bell et al. 2005), and there can be systematic overestimates of the SFR by a few tenths of a dex. In the next section we attempt to improve the SFR measurement by comparing IR and far-UV, stacking the MIPS images to get a median flux for non-MIPS-detected objects.

5.4.2. SFR from UV luminosity

We can also estimate the SFR from UV luminosity. At $z = 1.4$, our B and R filters are roughly at restframe 1800 and 2800 Å. We compute absolute AB magnitudes at 1500 and 2200 Å using our SED K-correction procedure, and compute the slope β of the UV continuum, $f_\lambda \propto \lambda^\beta$. The UV slope has been used as an indicator of extinction by Meurer et al. (1999), who found a far-UV extinction at 1500 Å: $A_{FUV} = 4.43 + 1.99\beta$ for local starburst galaxies. This relation may vary depending on galaxy type; Bell (2002) found that local normal galaxies deviate to lower A_{FUV} . Large samples of local galaxies studied in the UV with GALEX suggest that applying the Meurer et al. (1999) prescription can overestimate A_{FUV} (Seibert et al. 2005; Treyer et al. 2007; Salim et al. 2007).

Although our $z = 1.4$ sample is selected at 2800 Å and is forming stars rapidly, it is not clear that local starbursts are the best approximation as these are a highly selected sample. We computed FUV attenuation using the relation $A_{FUV} = 3.16 + 1.69\beta$ (Seibert et al. 2005, as updated by Treyer et al. 2007). We correct the FUV luminosity and compute an SFR following Kennicutt (1998), scaled by 0.7 to convert from a Salpeter to Kroupa IMF for consistency with the SFR(IR) estimate:

$$SFR(FUV)(M_\odot \text{ yr}^{-1}) = 1.0 \times 10^{-28} L_\nu(1500 \text{ Å})(\text{erg/s/Hz}). \quad (4)$$

The A_{FUV} prescription of Salim et al. (2007) yields nearly identical SFR, while the prescription of Meurer et al. (1999) yields SFRs 0.4 dex higher. The accuracy is limited since there is substantial scatter about the $A_{FUV} - \beta$ relation, 0.9 mag in the Seibert et al. (2005) sample. The median values and $\pm 34\%$ range for β and A_{FUV} in our no-excess-emission galaxy sample are -0.65 ± 0.42 and 2.06 ± 0.71 respectively. The UV continuum slope is correlated with magnitude and restframe color - brighter, redder, more massive galaxies have redder UV continua.

Figure 11 shows a comparison of SFR estimates from the far-IR and from the far-UV with the Seibert et al. (2005) $\beta - A_{FUV}$ relation, for 194 galaxies in the Mg II sample and MIPS imaging area. For galaxies not detected by MIPS, we set an upper limit based on the 4σ limit at 24 μm of 65 μJy .

Because many of the galaxies are not individually detected by MIPS, we divided the FUV sample into three ranges at the 25 and 75th percentiles. For those galaxies with MIPS imaging, we then median stacked the MIPS 24 μm images. This yields a good detection in all three ranges. The median SFR(IR+UV) for the three ranges is plotted against the median SFR(FUV) as the large circles in Figure 11.

The SFR(FUV) following Seibert et al. (2005) is in good agreement with the SFR(IR); it is 0.1 dex low for the more rapidly star-forming galaxies. The Meurer et al. (1999) prescription for A_{FUV} yields SFRs 0.4 dex higher than the Seibert A_{FUV} , and would overestimate SFR by ~ 0.3 dex for this sample. We adopt the SFRs derived from the Seibert A_{FUV} and plot them in Figure 12. These galaxies are on average higher SFR, more IR-luminous, and can be more extinguished than the local samples for which the UV relations were defined. However, the stacked-IR to UV comparison allows us to infer an SFR for all galaxies in the sample that is consistent with mid-IR determinations, even though only a small number of the galaxies have individual mid-IR measurements. As

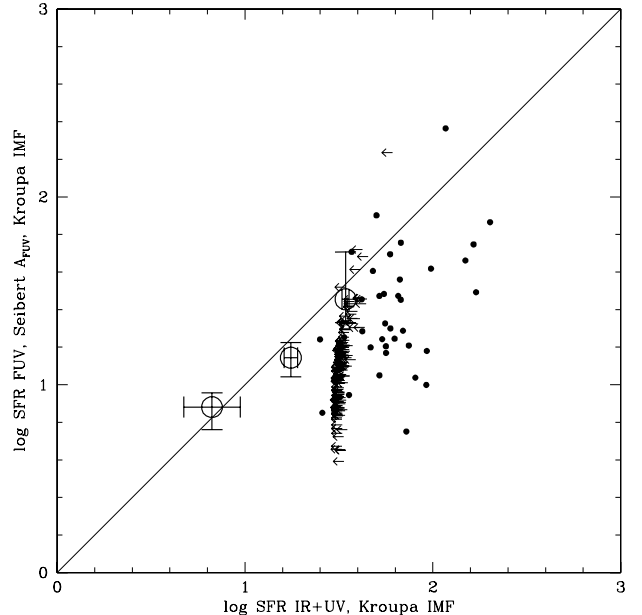


FIG. 11.— Comparison of star formation rates inferred from 24 μm + UV, and from far-UV luminosity with the Seibert et al. (2005) relation for A_{FUV} , for 194 galaxies in the Mg II sample with MIPS imaging. Calibrations refer to a Kroupa IMF. Leftward-pointing arrows are upper limits for galaxies not detected by MIPS. The large open circles show the median SFR(FUV) for galaxies subdivided into three ranges of L_{FUV} , and the SFR(IR+UV) derived by a median stacking of their MIPS 24 μm images.

with the mid-IR measurement, AGN luminosity could contribute to the far-UV, but only a small fraction of the galaxies have evidence for an AGN, based on Mg II emission. In addition, of the sample galaxies in the EGS field, very few are detected in X-rays (Nandra et al. 2007).

The stacked MIPS detections imply that the galaxies in the $< 25\%$ ile, 25 – 75%ile, and $> 75\%$ ile of SFR(FUV) have median IR luminosities $L_{IR}(8 - 1000\mu\text{m}) = 3.1 \times 10^{10}$, 1.3×10^{11} , and $2.5 \times 10^{11} L_\odot$ respectively, and median SFRs of 7, 18, and 34 $M_\odot \text{ yr}^{-1}$. The median galaxy in the $z \sim 1.4$ Mg II sample is roughly at the LIRG threshold of $L_{IR} = 10^{11} L_\odot$.

5.5. Correlation of galaxy properties with SFR

Figure 10 plots galaxy magnitudes, stellar mass, and color against each other, and Figure 12 compares magnitude and stellar mass estimates against star formation indicators. Because the sample is selected at restframe 2800 Å, color, M_B and stellar mass are highly covariant. The color-magnitude plot shows that the sample contains blue galaxies at a range of luminosities, but few red-sequence galaxies; red galaxies are disfavored by the UV selection and their lower abundance at $z > 1$ (Willmer et al. 2006). SFR as estimated from the UV is strongly correlated with M_B but somewhat less well with stellar mass: galaxies with high extinction-corrected FUV luminosity are fairly high-mass. The SFRs are for a Kroupa IMF while the stellar masses are normalized to a Chabrier IMF, which is just slightly lower.

Note that the SFR_{FUV} correlates fairly tightly with M_B , more so than with other quantities; SFR_{FUV} is less tightly correlated with UV luminosity itself. This is caused by the extinction correction - the UV slope and $UV - B$ color are highly correlated (see also Treyer et al. 2007). The correla-

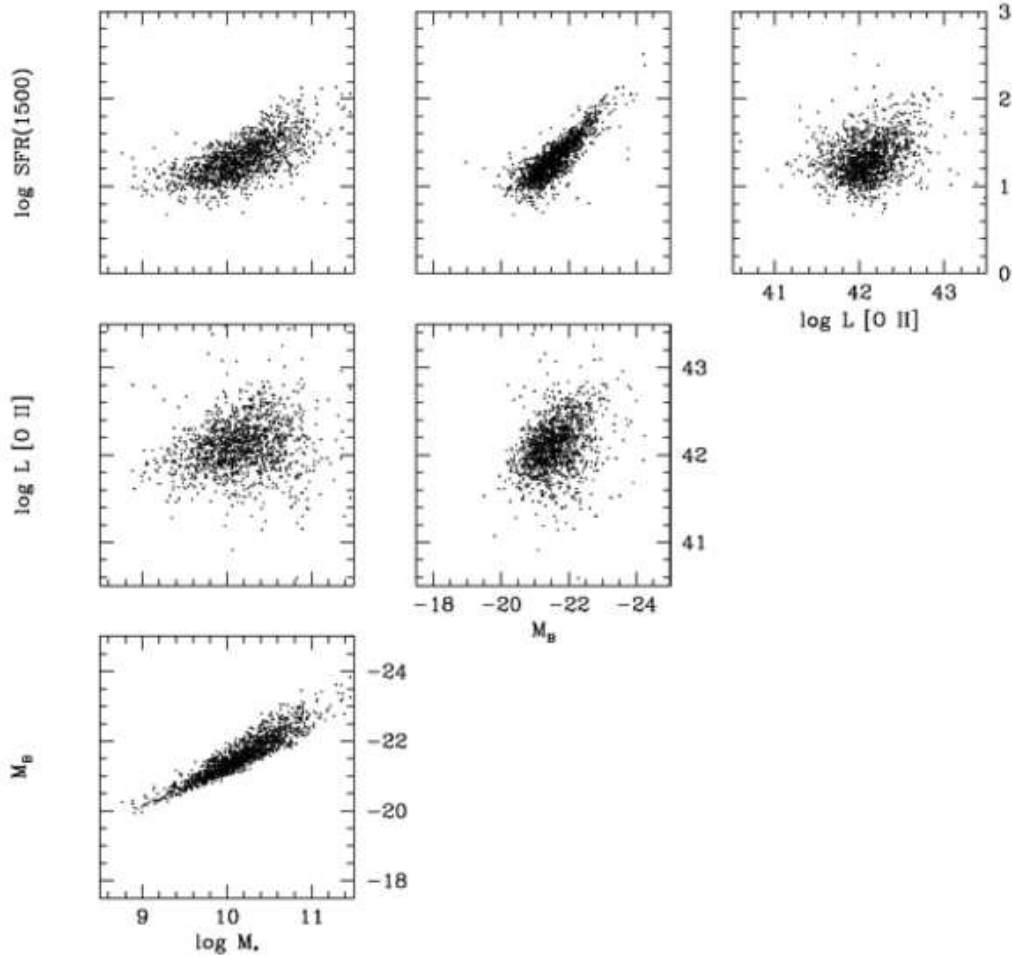


FIG. 12.— Blue magnitude and stellar mass compared to [O II] luminosity in erg/sec, and star formation rate estimated from the FUV luminosity in $M_{\odot} \text{ yr}^{-1}$. The SFR(FUV) is corrected for extinction and the [O II] luminosity is not. The extinction correction causes M_B and $SFR(FUV)$ to be highly correlated.

tion is also partially induced by the K-correction procedure since we have to infer M_B from restframe U and color. If the sample included red non-starforming galaxies, they would fall to lower SFR, below the correlation.

The velocity linewidth σ of the [O II] emission is correlated with magnitude and stellar mass, with considerable scatter. Much of this scatter is due to the large scatter in the high-redshift linewidth Tully-Fisher relation (Weiner et al. 2006), which may be induced both by inclination and by details of the internal kinematics. Velocity width and SFR are essentially uncorrelated, largely due to scatter in the estimators.

6. OUTFLOW DEPENDENCE ON GALAXY PROPERTIES

To study how galaxy properties affect the outflow, we divide the no-excess-emission sample into subsamples binned in either magnitude, stellar mass, or star formation rate in turn, and coadd the spectra with these bins. We choose the bin limits to separate the bottom 25%, middle 25%-75%, and top 25% in each property.

6.1. Outflows exist across the range of luminosity, mass, and SFR

The panels of Figure 13 show the coadded spectra at Mg II for subdivisions in M_B , M_* , and $SFR(FUV)$ respectively. Table 1 summarizes the results of the decomposition into symmetric and outflow absorption, and the [O II] emission in each coadded spectrum.

The symmetric absorption is strongly dependent on the properties, being much weaker in the low-mass, low-SFR end of the sample. The dispersion of the symmetric Mg II absorption varies more strongly than the velocity dispersion of [O II]; it is high in redder/more massive objects. These objects contain a cooler stellar population, with stronger and broader photospheric Mg II absorption (as in e.g. the models of Rodríguez-Merino et al. 2005), so that the dispersion reflects stellar properties. Note that there is almost no absorption at zero velocity in the bluer, lower-mass, lower-SFR subsample. This is surprising since internal absorption by the galaxies' ISM should occur, on average, at zero velocity, and even low columns of cool gas produce Mg II. It appears that in the lower-mass galaxies *all* of the cool gas between us and the UV-emitting stars is outflowing.

The outflow component of the absorption exists in all subdivisions of the sample. Its equivalent width is higher in the

brighter, redder, high-mass, high-SFR subdivisions – since all of these galaxy properties are correlated, it is not possible to isolate one parameter that predicts outflow strength much better than the others. Although the blueshifted absorption is stronger in the larger galaxies, it is still fairly strong in the smaller, low-mass galaxies. We have not found any class of galaxy in the sample that does not exhibit outflow absorption, justifying the claim above that the Mg II outflows are ubiquitous in the DEEP2 sample. Although this sample is selected to all be fairly luminous at restframe 2800 Å, it covers a range of $10\times$ in SFR and B luminosity, and $30\times$ in stellar mass.

We quantify the velocity extent of the outflow absorption in two ways: the median velocity of absorption, V_{med} , and the velocity where outflow-component absorption reaches a threshold depth. We lightly smooth the outflow absorption spectrum A_{flow} with a boxcar of 5 pixels (68 km s^{-1}) to reduce noise, and count from -100 km s^{-1} downward to more negative velocities until reaching a pixel that is above 0.75 or 0.9 of the continuum value. These velocities define the locations $V_{25\%}$ and $V_{10\%}$, respectively, the extent of contiguous 25% or 10% absorption depth. These threshold measurements are more robust than attempting to measure a maximum outflow velocity, since in the composite spectra, the outflow absorption is not a set of discrete components, but gradually asymptotes to zero at high velocities.

Figure 14 overplots the absorption components of the three subsamples in mass and SFR, demonstrating that the high-mass and high-SFR subsamples show greater absorption at $-800 < V < -400 \text{ km s}^{-1}$ than the intermediate and low-mass or -SFR subsamples. The velocity extents of outflow are tabulated in Table 1 and plotted in Figures 15 and 16.

Both the depth of the outflow absorption and its velocity extent are greater for the brighter, high-mass, high-SFR, redder-color fractions of the sample. This is similar to the trend found by Shapley et al. (2003) in $z \sim 3$ Lyman-break galaxies, where low-ionization lines are stronger in the galaxies with higher SFR, larger velocity offset, and redder UV continuum slope. Fitting a power-law dependence of the velocity of the 10% absorption depth, $V_{10\%}$, on mass or SFR, yields $V_{10\%} \propto M_*^{0.17}$ and $V_{10\%} \propto SFR_{FUV}^{0.38}$. The power-law slopes for $V_{25\%}$ are 0.11 and 0.17 on M_* and SFR_{FUV} respectively. These measures are dependent on the choice of the absorption threshold, but it appears that that $V_{wind} \sim SFR_{FUV}^{0.3}$. It is suggestive that the velocity appears to have a stronger dependence on SFR than on stellar mass, but this could be because our sample spans a larger range in stellar mass than it does in SFR. Notably, the $z = 1.4$ starforming galaxies have a similar dependence of wind velocity on SFR to the low- z ULIRGs studied by Martin (2005) in Na I, who found an upper envelope of wind velocity at $V \sim SFR^{0.35}$.

6.2. Search for outflow dependence on galaxy type

Locally, starburst-driven winds are more frequently seen in face-on galaxies, due to collimation of biconical outflows (Heckman et al. 2000; Rupke et al. 2005b). 118 of the Mg II sample galaxies are in the Extended Groth Strip and have HST ACS I -band imaging (Davis et al. 2007; Lotz et al. 2008). We divided them up by axis ratio as measured with SExtractor (Bertin & Arnouts 1996) in an attempt to separate face-on and edge-on galaxies. We did not find a correlation between axis ratio and wind strength or wind velocity. An examination of the ACS images shows that the galaxies are too irregular and low surface brightness to trust the axis ratio as a measure of

disk inclination. Many may not be disks. Because the imaging is at restframe U -band, the high- z galaxies are more irregular, and their images appear to be highly affected by starforming regions and by dust.

We also classified the galaxies by eye into six broad morphological types: face-on, edge-on, chain, irregular, merger, and compact, finding 37, 13, 18, 28, 3, and 19 respectively. The large number of chain, irregular and compact galaxies indicates that many $z = 1.4$ galaxies are not obviously disk in the rest U . When we coadd the spectra within each type, we find that all types exhibit blueshifted Mg II absorption – even the 3 mergers have enough signal to detect it. However, the noise in the spectra and the variance among individual objects within a type prevent us from determining whether the outflows in one type are stronger than another. Note however that the merger fraction is low, as is true of $z \sim 1$ galaxies in general (Lotz et al. 2008). While many galaxies are irregular or disturbed, major mergers are not a prerequisite for driving a wind in this sample.

In the ACS imaging, the median of the galaxies’ Petrosian radii is 5.2 kpc and there is a weak correlation between size and magnitude, and no obvious correlation between size and outflow. These tests show that winds are found across all star-forming types at $z = 1.4$, but they neither prove nor disprove collimation of winds in this sample. A larger number of galaxies with HST near-IR imaging, and spectra at Mg II, are needed to search for collimation and morphological type dependence.

7. ANALYSIS AND DISCUSSION

7.1. Physical properties of the outflow

The amount of gas contained in the outflows is of great interest in gauging its importance to galactic and IGM evolution. Because the Mg II lines are optically thick, approaching the “flat part” of the curve of growth, we cannot infer column density directly from the equivalent width. Here we use the classical doublet ratio method to approximate the optical depth and column density (Spitzer 1968; see also Jenkins 1986 and Rupke et al. 2005a).

The EW ratio of the two Mg II lines, W_{2796}/W_{2803} , varies from 2 to 1 for optical depth τ from 0 to infinity. For a single absorber, there is a relation between the EW ratio and the optical depth at line center τ_0 (C in the notation of Spitzer 1968, Table 2.1). For an ensemble of absorbers, the relation does not strictly apply, but generally yields accurate results in the mean if the saturation is not too strong (Jenkins 1986). The doublet ratio is given by $F(2\tau_0)/F(\tau_0)$ where F is the integral of transmission over the line, and the column density in atoms cm^{-2} is (Spitzer 1968):

$$\log N = \log \frac{W_{2803}}{\lambda} - \log \frac{2F(\tau_0)}{\pi^{1/2}\tau_0} - \log \lambda f_{2803} + 20.053. \quad (5)$$

We computed EWs for the Mg II lines in the outflow components of the no-excess-emission sample (1356 galaxies), and in the subsamples split by stellar mass and SFR. We compute the EW between 0 and -768 km s^{-1} for each line, and exclude above-continuum pixels to eliminate those most grossly affected by emission. These EWs and the inferred optical depths are tabulated in Table 2. The formal errors on the EWs are small, but the systematics are significant due to (1) underlying Mg II emission, which tends to decrease W_{2803} and overestimate the true ratio; and (2) limits on the applica-

TABLE 1
ABSORPTION AND EMISSION PROPERTIES OF CO-ADDED GALAXY SAMPLES

category	# of galaxies	Symmetric absorption ^a		Outflow absorption ^a				[O II] emission ^c	
		W_{2803} , Å	σ^b , km s ⁻¹	W_{2796} , Å	V_{med}	$V_{25\%}$	$V_{10\%}$	EW ^d , Å	σ^b
All, Mg II	1406	0.61 ± 0.03	64.7 ± 4.1	1.71 ± 0.06	-279 ⁺¹⁷ ₋₉	-364	-515	44.3	68.7
All, Mg I	1406	0.32 ± 0.04	106.0 ± 15.9	0.58 ± 0.05	-194 ⁺³³ ₋₁₉	...	-299	44.3	68.7
MIPS 24 μm sources	37	0.64 ± 0.12	69.6 ± 16.2	1.70 ± 0.22	-311 ⁺⁵⁹ ₋₃₇	-501	-584	30.2	67.6
$M_B > -21.15$	339	0.14 ± 0.05	0.0	1.49 ± 0.16	-266 ⁺³⁶ ₋₄₉	-419	-474	64.2	59.1
$-21.15 < M_B < -21.96$	678	0.85 ± 0.05	70.2 ± 5.4	1.45 ± 0.10	-226 ⁺²⁴ ₋₂₃	-336	-405	47.9	69.6
$M_B < -21.96$	339	1.44 ± 0.07	122.0 ± 6.7	1.96 ± 0.10	-315 ⁺³³ ₋₁₀	-405	-639	31.1	76.2
$\log M_* < 9.88$	339	0.08 ± 0.04	0.0	1.39 ± 0.14	-269 ⁺⁴³ ₋₃₇	-295	-446	63.2	60.3
$9.88 < \log M_* < 10.45$	678	1.08 ± 0.06	91.3 ± 5.9	1.55 ± 0.10	-246 ⁺³⁴ ₋₈	-336	-515	50.2	69.6
$\log M_* > 10.45$	339	1.33 ± 0.07	104.7 ± 7.6	1.91 ± 0.12	-309 ⁺²³ ₋₂₇	-377	-653	27.6	76.7
$\log SFR < 1.15$	339	-0.13 ± 0.30	0.0	1.46 ± 0.15	-233 ⁺⁴³ ₋₃₂	-295	-432	60.1	60.2
$1.15 < \log SFR < 1.45$	678	1.08 ± 0.06	90.2 ± 6.4	1.43 ± 0.11	-256 ⁺³⁰ ₋₂₁	-336	-446	47.2	69.0
$\log SFR > 1.45$	339	1.34 ± 0.06	111.8 ± 6.2	1.84 ± 0.10	-290 ⁺¹⁰ ₋₃₂	-364	-653	33.3	75.0

^a Symmetric and outflow absorption are measured for Mg II 2803 and 2796 Å, respectively, except for the “All, Mg I” sample, where they are for Mg I 2852 Å. Absorption EWs are for the 2796 Å line of the Mg II doublet; the total is approximately twice as large.

^b Corrected for $\sigma_{inst} = 25$ km s⁻¹. Symmetric absorption lines in the faint/blue quartile are consistent with zero intrinsic width.

^c Statistical errors on [O II] emission are 0.5 – 1 Å in EW and 0.5 – 2 km s⁻¹ in σ .

^d [O II] emission EW is the total of both lines in the doublet.

TABLE 2
MG II EQUIVALENT WIDTH AND DOUBLET RATIOS

category	W_{2796}^a , Å	W_{2803}^a , Å	Ratio	τ_0
no excess emission	1.54	1.37	1.13	~ 8 – 10
$\log M_* < 9.88$	1.24	1.26	0.98 ^b	> 10
$9.88 < \log M_* < 10.45$	1.55	1.41	1.10	~ 10 – 20
$\log M_* > 10.45$	1.73	1.48	1.17	~ 5
$\log SFR < 1.15$	1.49	1.25	1.19 ^b	~ 5
$1.15 < \log SFR < 1.45$	1.37	1.31	1.04	> 10
$\log SFR > 1.45$	1.67	1.47	1.14	~ 8

^a EW is computed only between 0 and -768 km s⁻¹ and excludes above-continuum pixels.

^b Most strongly affected by emission.

bility of the simple doublet ratio method. Given systematics, there are no significant differences between the subsamples in doublet ratio or in optical depth.

Generally, the doublet ratios derived are 1.1 to 1.2, or even lower. Adjusting the velocity interval has little effect. Computing the ratio directly on the observed spectrum, rather than the wind component only, yields lower doublet ratios, around 1.0.

For doublet ratios 1.20 – 1.10, the optical depths are $\tau_0 = 4 - 20$, and $F(\tau_0)/\tau_0 = 0.33 - 0.093$, so there is a factor of ~ 3.5 range in inferred column density. To get a characteristic column density of the outflow, we take typical values $W_{2803} = 1.37$ Å and $\tau_0 = 10$, with $\log \lambda f = 2.933$ (Morton 1991). The inferred column density is $\log N_{MgII} = 14.5$ atoms cm⁻². The optical depths derived here, $\tau_0 \sim 4 - 20$, range high enough that the results of Jenkins (1986) may not apply and the inferred column densities could be *underestimated*.

To be conservative, we make no ionization correction; Mg I is present but relatively weak. The presence of Mg I in the outflow, with ionization potential 7.7 eV, suggests some amount of cold gas and/or shielding from UV radiation. The Mg I line has a similar profile to Mg II, but the Mg I is not as deep. Mg I could be weaker due to lower column density or lower covering fraction. Because Mg II is saturated and Mg I has a higher oscillator strength than Mg II, getting the

observed Mg I by lowering the column requires fine-tuning the Mg I/Mg II ratio to a precise value to obtain unsaturated absorption. A more likely explanation is that Mg I is saturated but has lower covering fraction than Mg II; similarly we found a higher covering fraction for Mg II than Rupke et al. (2005b) find for Na I in low-redshift outflows. A modeling of the Mg II, Mg I, and incident UV field is beyond the scope of this paper, but could yield interesting constraints on wind physics (cf. Murray et al. 2007).

Assuming a solar abundance ratio of $\log \text{Mg}/\text{H} = -4.42$ and an Mg depletion of -1.2 dex, typical in the local ISM (Savage & Sembach 1996) and reasonable for outflows given that local outflows in luminous galaxies are dusty (Heckman 2002), the inferred atomic column density is $N_H = 1.3 \times 10^{20}$ atoms cm⁻². The average galaxy in the DEEP2 $z \sim 1.4$ sample is expelling and covered by at least a sub-damped Lyman-alpha absorber’s worth of outflowing gas. This column density is integrated over viewing angle and clumpiness of absorbers, so it includes the covering fractions C_Ω and C_f . The column density is moderately lower than the columns of $\sim 10^{21}$ atoms cm⁻² inferred from Na I in low-redshift infrared-luminous galaxies (Heckman et al. 2000; Rupke et al. 2005b). Our estimate is conservative in the optical depth and lack of ionization correction, and possible effects of highly saturated Mg II, while those authors have had to apply a large ionization correction for Na I, so the measurements are essentially consistent.

The IR luminosities of the Heckman sample are roughly comparable to the DEEP2 galaxies, while the Rupke sample is at higher L_{IR} in the mean, since only half of the DEEP2 galaxies would be LIRGs. The major difference is frequency of occurrence: the Heckman and Rupke samples are relatively special objects locally, while the DEEP2 sample represents a broad range of the luminous star-forming objects at $z \sim 1.4$, where the global SFR is higher. This reflects the overall higher SFR of individual galaxies at high redshift (e.g. Le Floc’h et al. 2005; Noeske et al. 2007a), but there may also be differences in the physical properties of the objects, compared further in Section 7.3.

The column density, velocity and a characteristic size allow

an estimate of the typical mass outflow rate. For a single thin shell wind at radius R , thickness $d \ll R$, outflow velocity v , with angular covering fraction C_Ω , clumpiness covering fraction C_f , and mean atomic weight μm_p ,

$$\dot{M} = 4\pi C_\Omega C_f \mu m_p N_H R v, \quad (6)$$

while for a thick wind that extends from radius 0 to R ,

$$\dot{M} = \frac{4\pi}{3} C_\Omega C_f \mu m_p N_H R v. \quad (7)$$

For a composite spectrum of galaxies viewed at all angles, the composite integrates over covered and uncovered lines of sight and clumpiness within the outflow, so we set $C_\Omega C_f = 1$. The sizes of the outflows are not easily constrained but must be at least of order the galaxy radius, since the covering factor is large. In our sample, the median Petrosian radius for galaxies with ACS imaging is 5.2 kpc and the 50% outflow velocity is 279 km s⁻¹. For a thin shell geometry and using typical numbers, with $\mu = 1.4$:

$$\dot{M} \simeq 22 M_\odot \text{ yr}^{-1} \frac{N_H}{10^{20} \text{ cm}^{-2}} \frac{R}{5 \text{ kpc}} \frac{v}{300 \text{ km s}^{-1}}. \quad (8)$$

This mass outflow rate is similar to the galaxies' star formation rates of 10–100 $M_\odot \text{ yr}^{-1}$, supporting the idea that galactic winds powered by star formation and the resultant supernovae drive an outflow of $\dot{M} \sim \text{SFR}$ (e.g. Heckman et al. 2000; Pettini et al. 2000; Heckman 2002; Veilleux et al. 2005). A mass outflow rate roughly equal to the SFR, fueled by continuing accretion, can help explain trends of SFR and metallicity in high-redshift galaxies (Erb 2008). The star formation rate, characteristic velocity, and outflow EW are all higher in the more massive/luminous objects in our sample, so the mass outflow in large galaxies is substantial.

A critical unknown is the radial extent that the outflow reaches. Some dramatic instances of superwinds in local galaxies that reach large distances are seen in X-ray and H α imaging (e.g. Strickland et al. 2004). It is well known that Mg II QSO absorption line systems occur within ~ 50 kpc of luminous galaxies, and also that luminous galaxies have a large covering factor within that radius, possibly dependent on galaxy type (e.g. Lanzetta & Bowen 1990; Bergeron & Boisse 1991; Steidel, Dickinson & Persson 1994; Bowen, Blades & Pettini 1995; Chen & Tinker 2008). However, whether these systems are mostly related to galactic outflows is debated (e.g. Bond et al. 2001; Steidel et al. 2002; Prochter, Prochaska, & Burles 2006; Bouché et al. 2006; Kaprczak et al. 2007; Tinker & Chen 2008). From these examples, it is suggestive, but not definitive, that the Mg II outflows could reach large distances, tens of kpc or more. In the next section we use outflow velocities to discuss whether the gas can escape.

7.2. Can winds escape from galaxies?

Galactic winds are the prime suspect for the enrichment of the intergalactic medium. The widespread detection of metals in intergalactic and intracluster gas reveals that, somehow, gas must get out of galaxies. The details of this process are difficult to model, and a number of treatments have come to different answers on the significance of gas and metal escape as a function of galaxy mass. Some have favored gas escape from the shallower potential wells of small galaxies and dark halos (Larson 1974; Dekel & Silk 1986) while others suggest

that the ISM dynamics and loading of cool gas into the wind are more important than the depth of the potential (De Young & Heckman 1994; Strickland & Stevens 2000).

Here the best probe we have is to compare the wind velocity to the galaxy escape velocity; we assume that the observed high velocity wind gas has already punched out of the disk or densest regions of the ISM, since its global covering fraction is significant.

To estimate the galaxy escape velocity, we scale the [O II] emission linewidths σ , which are an estimator of the circular velocity V_c . For a halo with outer radius r_h and a flat rotation curve, the escape velocity at R is $V_{esc}(R)^2 = 2V_c^2 \ln(1 + r_h/R)$ (Binney & Tremaine 1987). For reasonable halo mass distributions, $V_{esc} \simeq 3V_c$, and is only weakly dependent on the outer radius r_h . The line-of-sight emission linewidths are related to the rotation velocity by $\sigma \sim (0.5 \text{ to } 0.6)V_c$, where σ incorporates an average over inclinations, as observed, but V_c is the true value (Rix et al. 1997; Kobulnicky & Gebhardt 2000; Weiner et al. 2006). There is scatter in this relation of $\sim 25\%$; in the mean it implies that

$$V_{esc} \simeq (5 \text{ to } 6) \times \sigma([\text{O II}]). \quad (9)$$

To be conservative we have used the high factor of 6 in computing V_{esc} for Figures 15 and 16. These figures show V_{esc} based on the composite [O II] linewidth and the median and $\pm 34\%$ range of V_{esc} based on the individual linewidth measurements of galaxies in each subsample. Errors on the linewidths tend to broaden the velocity distribution. The threshold velocity where Mg II absorption reaches 10%, $V_{10\%}$, is moderately higher than median V_{esc} in the subsamples of low and intermediate mass and SFR. However, in the high-mass or high-SFR subsample, $V_{10\%}$ is substantially more than the median V_{esc} estimated from the galaxy velocity widths. This effect is caused by the tail of high-velocity absorption shown in the high-mass, high-SFR subsamples in Figure 14.

The high velocities in the tail of the outflow distribution suggest that low-ionization gas is able to reach large radius or even escape. This could give rise to Mg II halo absorption systems, but more rigorous modeling of the EW distribution and covering factor will be necessary to confirm that. Prochter et al. (2006) have argued that the redshift evolution of the number of strong Mg II absorbers links them to the global SFR evolution and to starburst events in low-mass galaxies. However, statistical detections of the associated light and the dust content of Mg II absorbers suggest a link to outflows from massive galaxies (Zibetti et al. 2007; Ménard and Chelouche 2008).

Bouché et al. (2006) advocated an outflow origin (rather than kinematics governed by halo mass) for Mg II absorbers. This was based on an anti-correlation between absorber equivalent width (velocity spread) and host halo mass, derived from clustering statistics. However, we do find a correlation of outflow EW or velocity spread with galaxy mass. A more sophisticated treatment of the clustering based on halo occupation suggests that the absorber-halo mass relation is partly related to the shocking of cold gas in very massive halos (Tinker & Chen 2008). The ubiquity of Mg II outflows that we find and the correlation of SFR and outflow strength suggest that at least some fraction of Mg II absorbers arise in outflows from massive galaxies, but there is not yet a fully consistent link, and there could be multiple causes for Mg II absorbers.

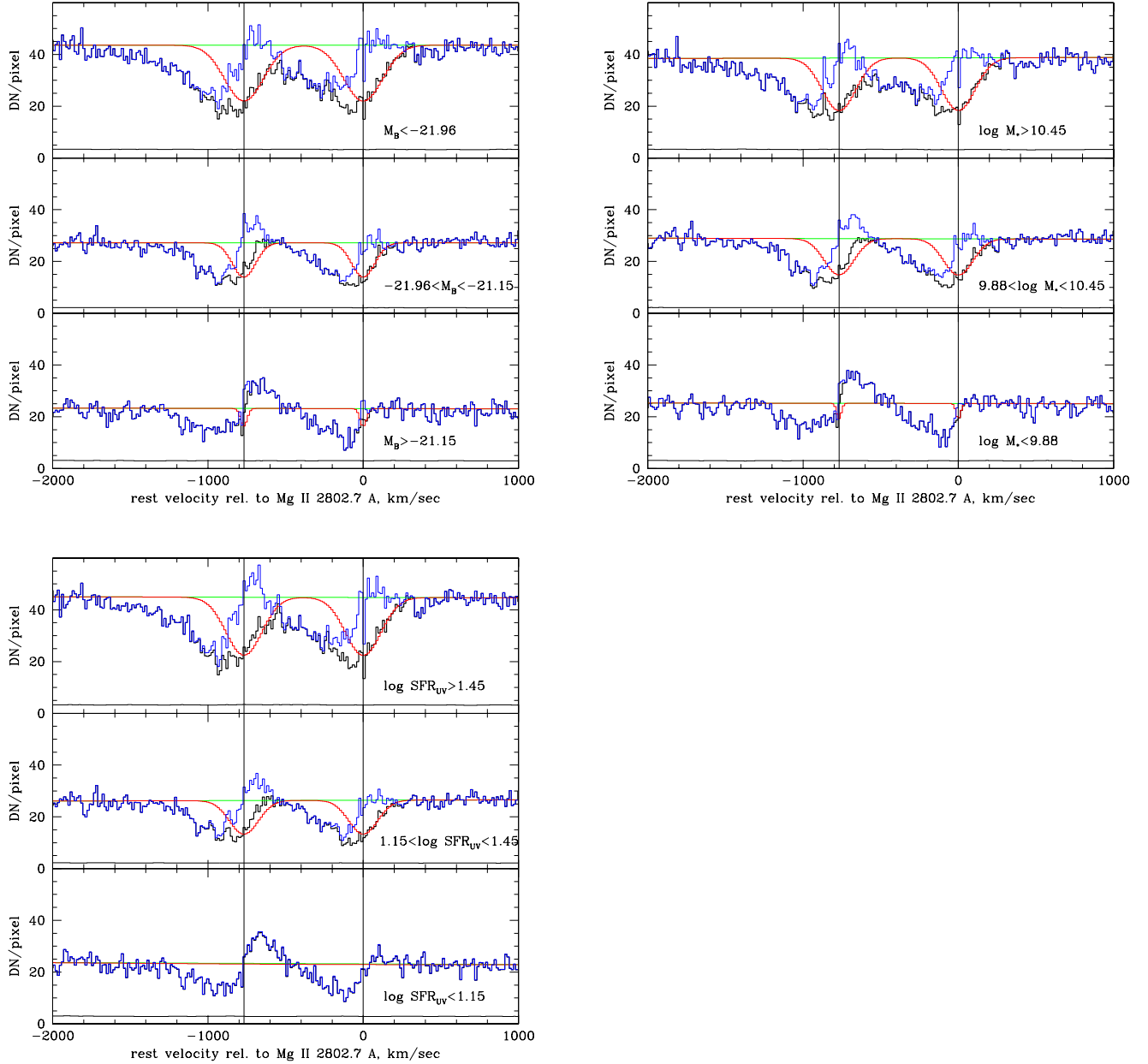


FIG. 13.— Mg II absorption for subsamples split by galaxy properties. In each panel, co-added spectra are shown for three subsamples, of low quartile, middle 50%, and high quartile. The subsamples are divided on: M_B absolute magnitude (upper left panel), M_* stellar mass (upper right), and SFR_{FUV} (lower left). The co-added spectra are decomposed into continuum (green straight line), symmetric absorption (red gaussians), and blueshifted absorption (blue asymmetric line), as in Figure 8.

7.3. Comparison to low-redshift winds and IR-luminous galaxies

Given the galaxies' range of SFR from $10\text{--}100 M_{\odot} \text{ yr}^{-1}$, and the median Petrosian radius of 5.2 kpc in the subset with ACS imaging, essentially all of the galaxies are above the criterion of $SFR > 0.1 M_{\odot} \text{ yr}^{-1} \text{ kpc}^{-2}$ where winds are typically found in the local universe (Heckman 2002). This suggests that the criterion also applies to high redshift galaxies, or conversely that it is no surprise that winds are ubiquitous in this sample. Because IR-luminous galaxies are more common at $z = 1$ (Le Floch et al. 2005) and the higher SFR at $z = 1$ occurs across the entirety of the starforming population (Noeske

et al. 2007a), in retrospect it might have been expected that winds should be common at $z > 1$.

Martin (2005) established in low- z ULIRGs that the upper envelope of the outflow velocity detected in Na I absorption depends weakly on SFR, $V_{wind} \sim SFR^{0.35}$. As noted above, we find a similar power-law exponent, $V_{wind} \sim SFR^{0.3}$, for the $z = 1.4$ star-forming galaxies, even though these are mostly well below ULIRG luminosities. Rupke et al. (2005b) found a wide dispersion of outflow velocities in galaxies with $SFR \gtrsim 100 M_{\odot} \text{ yr}^{-1}$, but a correlation between outflow velocity and SFR or V_c when both IR-luminous galaxies and dwarfs with winds are considered. Their sample shows a weak cor-

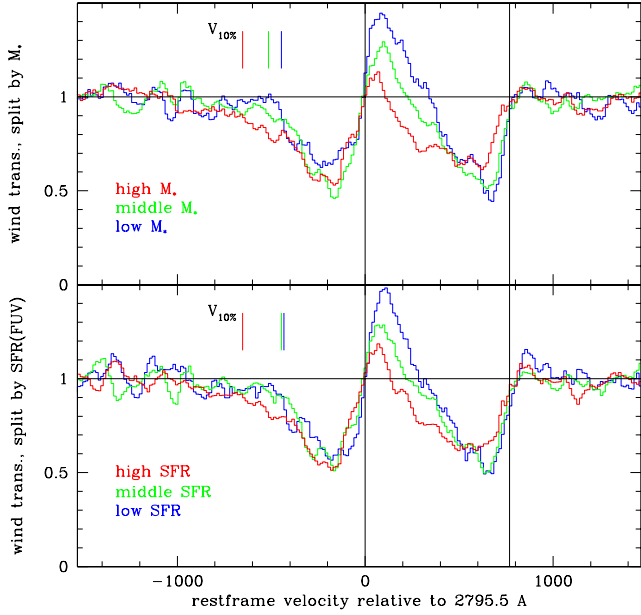


FIG. 14.— Mg II outflow absorption component $1 - A_{flow}$ compared for galaxies in (upper panel) the three subsamples of stellar mass; (lower panel) the three subsamples of SFR_{FUV} . Velocity is referred to Mg II 2795.5 Å. A 5 pixel boxcar smooth has been applied. In each panel, the red, green, blue lines are for high to low mass, or SFR. The vertical lines at -400 to -650 km s $^{-1}$ show the location of $V_{10\%}$, where the outflow crosses 10% absorption. The high mass and high SFR galaxies show greater outflow absorption at $-800 < V < -400$ km s $^{-1}$ than the lower mass or SFR samples.

relation of Na I column with SFR and galaxy mass. Sato et al. (2008) use spectra from DEEP2 to study outflows in Na I at $z \sim 0.6$, and find that the detection fraction of winds is significantly higher in $24 \mu\text{m}$ detected galaxies than in other similarly massive galaxies. The Sato et al. sample does show some signs of outflow in galaxies without ongoing star formation, a population we do not probe in this sample. Our results agree with the sense of these trends: higher SFR galaxies have deeper and faster outflow absorption.

Comparing the $z \sim 1.4$ sample to the low-redshift IR-luminous galaxies of Rupke et al. (2005b), the DEEP2 Mg II sample has SFR and L_{IR} more like Rupke’s IRGs ($L_{IR} > 10^{11} L_{\odot}$) than his ULIRGs; the median DEEP2 galaxy is just at the $10^{11} L_{\odot}$ threshold. However, the $z \sim 1.4$ galaxies are somewhat more likely to host winds and to have higher outflow velocities than the low-redshift IRGs. Our absorption depth for winds in DEEP2, 55%, corresponds to detection frequency times clumpiness covering fraction in the Rupke IRGs, which is lower at $C_{\Omega} C_f \simeq 0.2$. The velocity to which we detect winds is also higher. Rupke et al. attempt to define a maximum velocity of robustly detected absorption by v_{max} containing $\sim 90\%$ of the absorption and find the low- z IRGs have $v_{max} = 301^{+145}_{-98}$ km s $^{-1}$. For comparison, we find that the velocity containing 50% of absorption V_{med} is often 250–300 km s $^{-1}$ (Table 1), suggesting that v_{max} is much higher. We find that at 10% absorption depth, $V_{10\%} = 400$ to 650 km s $^{-1}$.

Rupke et al. (2005b) find almost no absorbers at > 600 km s $^{-1}$ in star-formation dominated galaxies, and we find significant column at that velocity. It is quite possible that this comes from the difference between Na I and Mg II as tracers.

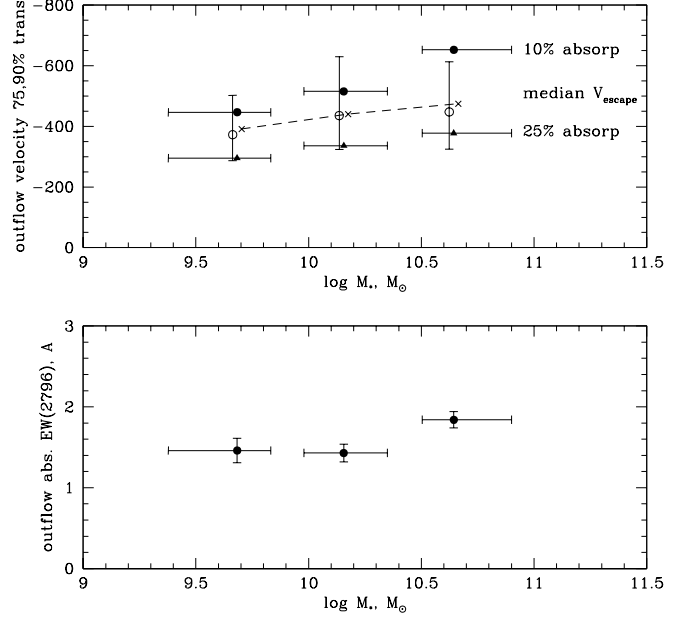


FIG. 15.— Upper panel: the outflow velocity at which wind Mg II absorption is 10% and 25% of continuum, for coadded spectra in three bins of stellar mass (filled points). The filled circles and horizontal error bars show the median and $\pm 34\%$ range of galaxies in the mass bin. The open circles and vertical errorbars are the median and $\pm 34\%$ range of escape velocity computed from the [O II] linewidth of galaxies in that bin, $V_{esc} = 6\sigma([\text{O II}])$. The Xes are the average escape velocity from the [O II] dispersion in the coadded spectrum. Lower panel: the EW of outflow Mg II absorption in the coadded spectra in three bins of stellar mass.

With its higher ionization potential, Mg II should be easier to find in low column density gas. We also find that Mg II is close to fully saturated, with a doublet ratio of 1.1 or even lower, while low- z Na I studies find somewhat less saturated absorption at ratios 1.2–1.3 (Heckman et al. 2000; Rupke et al. 2005b).

The Mg II study of very luminous post-starburst galaxies at $z \sim 0.6$ by Tremonti et al. (2007) found discrete absorbers at significantly higher outflow velocities than in our sample, often above 1000 km s $^{-1}$. Those galaxies, being post-starbursts are rather different from our sample and probably instances of AGN-driven rather than star formation driven winds. AGN-driven winds are expected to reach higher velocities than star formation-driven winds observationally and theoretically (Veilleux et al. 2005; Scannapieco & Oh 2004; Thacker et al. 2006).

Heckman et al. (2000) found relatively little dependence of the outflow speed on host galaxy V_c , using a mix of Na I and X-ray temperature measurements to obtain wind speed. This result suggested that gas preferentially escapes from low-mass galaxies. In contrast, in the $z \sim 1.4$ sample, we do find a dependence of outflow speed on galaxy mass, possibly due to the more uniform use of Mg II as an outflow probe and the more homogeneous galaxy sample (versus the local samples which tend to comprise IR-luminous galaxies and dwarfs with few intermediate objects).

Rupke et al. (2005b) suggested that gas could escape from ULIRGs, and thus that massive galaxies at high redshift influence the IGM; deep potentials do not inhibit wind formation. Martin (2005) also suggested that the dependence of velocity

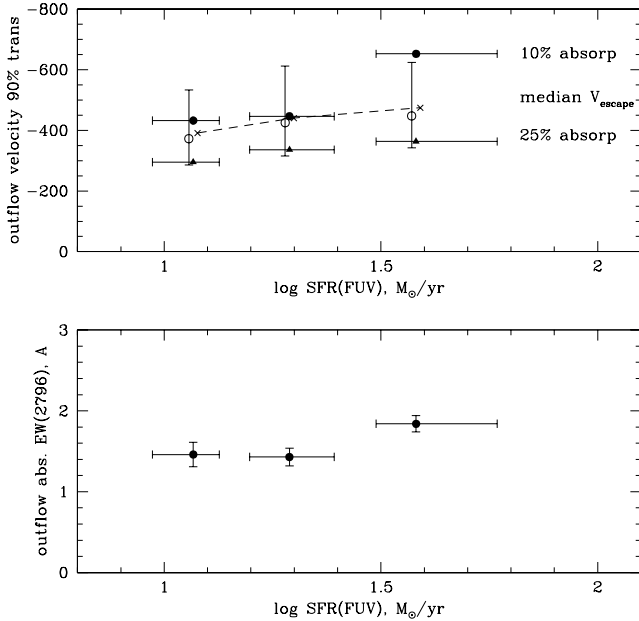


FIG. 16.— As Figure 15, but for SFR(FUV). Upper panel: outflow velocity at which wind Mg II absorption is 10% and 25% (filled circles) in three bins of SFR(FUV). The open circles and vertical error bars are the median escape velocity $V_{\text{esc}} = 6\sigma([\text{O II}])$, and the Xes are the average V_{esc} from the coadded [O II] linewidth. Lower panel: EW of outflow Mg II absorption in three bins of SFR(FUV).

on SFR implies that wind feedback is important in high mass galaxies. Our finding of outflow velocities at or greater than the escape velocity, and a greater effect in the high-SFR subsample, reinforces the point. A large fraction of the global star formation occurs in high-mass galaxies (e.g. Le Floch et al. 2005; Noeske et al. 2007b); if outflows scale positively with SFR, high-mass star forming galaxies have a significant impact on the enrichment and evolution of the IGM.

7.4. Implications for wind models and dependence on mass

These detections of the prevalence and properties of winds in starforming galaxies can constrain both the impact of winds on galaxies and the IGM, and the physical models of the wind mechanism.

Since the influential work of Larson (1974) it has been recognized that winds driven by supernovae could arise during galaxy formation and limit its progress. Larson suggested that these winds could cause more gas loss in smaller galaxies and explain the mass-metallicity relation. Subsequent treatments have emphasized the importance of winds for solving problems with low-mass galaxies in cold dark matter models of structure formation, such as reducing the number, luminosity, and metallicity of faint galaxies (e.g. Dekel & Silk 1986; Dekel & Woo 2003).

Hydrodynamical studies have shown that while it is relatively difficult for supernovae-driven outflows to clear low-mass galaxies entirely of gas, they can be fairly efficient at ejecting metals (De Young & Heckman 1994; Mac Low & Ferrara 1999). Star-formation driven winds are a necessary ingredient, under the name of “feedback,” for models of galaxy formation to reproduce observed scaling relations (e.g. Somerville & Primack 1999; Ceverino & Klypin 2007). Matching the observed radius, luminosity and velocity rela-

tions of disk galaxies requires that a large fraction of baryons either never make it into the disk or are blown out (Dutton et al. 2007).

Models of winds have tended to concentrate on the effect of winds on low-mass galaxies, where the question of complete gas blowout is more pressing, and where outflows are effective at leaving fossil evidence in the mass-metallicity relation (Garnett 2002; Tremonti et al. 2004; Dalcanton 2007). Star-formation driven outflows do not leave a strong trace in the metallicity of high-mass, low gas fraction galaxies, and so the mass-metallicity relation is not evidence against winds in high-mass galaxies (Dalcanton 2007). The baryonic Tully-Fisher relation does not show a break at low masses (Geha et al. 2006), as might be expected in models where winds are effective below a critical mass or circular velocity (e.g. Dekel & Silk 1986). Some models have predicted that the effect of winds is small in high-mass galaxies because the wind is blocked by gas within the disk (e.g. Dubois & Teyssier 2008; Dalla Vecchia & Schaye 2008).

But in fact, high-velocity winds in high-mass, SFR-dominated galaxies are demonstrated to exist in Lyman break galaxies (Shapley et al. 2003), in LIRG/ULIRGs (Rupke et al. 2005b; Martin 2005), and in blue-cloud starforming galaxies (this work). These could have significant effects on gas content, absorption-line systems, and the enrichment of the IGM and ICM, and so proper treatment of winds in high-mass galaxies is necessary to model these problems. Although winds probably have a stronger influence on the structure of low-mass galaxies than on high-mass galaxies, this does not tell us whether low- or high-mass galaxies are more important for IGM enrichment.

The behavior of winds in low and high mass galaxies is related to another theoretical problem, the appropriate physical model for the driving of the outflow. The cool gas in winds may be driven either by the kinetic energy of supernova ejecta, by entrainment in the hot wind (e.g. Chevalier & Clegg 1985; Heckman et al. 1990; Strickland & Stevens 2000) or by the momentum, through radiation pressure (Murray et al. 2005) or cosmic ray pressure (Socrates et al. 2006). These predict different scalings for the behavior of wind velocity with galaxy mass and SFR.

The observed X-ray temperature of winds varies little with galaxy mass, which would suggest relatively little dependence of cool gas velocity on galaxy mass (Martin 1999; Heckman et al. 2000). As pointed out by Martin (2005), the increase of wind velocity with SFR, $V \sim \text{SFR}^{0.35}$, which she finds in ULIRGs and we find across a broad range of starforming galaxies, is surprising if winds are energy-driven (though see Fujita et al. 2008). Momentum-driven winds appear to fit this scaling better (Murray et al. 2005), although a detailed comparison is beyond the scope of this paper.

We discuss one possible implication, the shape of the outflow absorption profile. In the momentum-driven wind model of Murray et al. (2005), cool gas is accelerated by radiation pressure, predicting $V^2(r) = 4\sigma_h^2(L/L_M - 1)\ln(r/r_0)$, where σ_h is the halo velocity dispersion and L_M is a critical luminosity to drive a wind. The radial dependence of the wind-driven cool gas density is not easy to predict, but it should decline with radius, e.g. $\rho(r) \sim r^{-2}$ to r^{-3} .

Figure 17 shows a toy model of the absorption that such a wind might produce (upper panel) for $\sigma_h = 150 \text{ km s}^{-1}$ and a 60% covering factor, to be compared with the Mg II outflow (lower panel). We have simply convolved the equations for

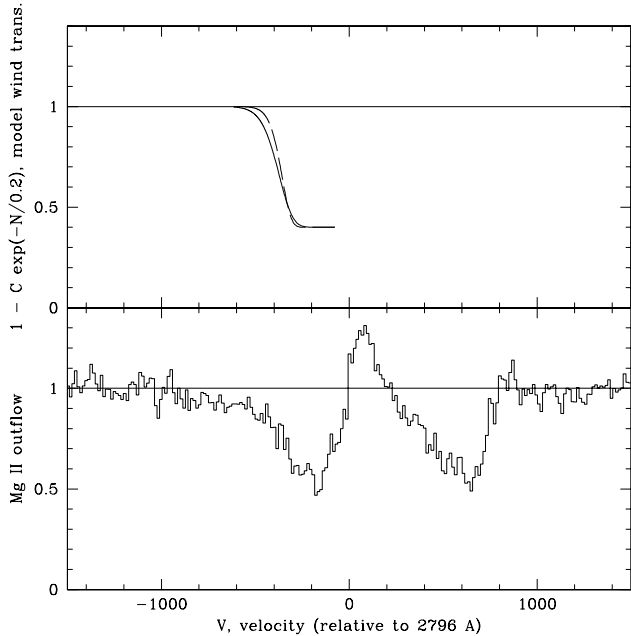


FIG. 17.— Upper panel: Absorption profile predicted by a model in which the gas is accelerated, with $v(r)$ increasing and $\rho(r)$ decreasing (e.g. Murray et al. 2005). The optical depth and covering factor have arbitrary normalization; the covering factor is 60%. The solid line is for $\rho \propto r^{-2}$ and the dashed line for $\rho \propto r^{-3}$. This model can produce an asymmetric profile. Lower panel: Observed Mg II outflow component profile, velocity relative to 2795.5 Å, in the no excess emission sample, with an asymmetric tail to high outflow velocity.

$V(r)$ and $\rho(r)$, assuming that the total covering factor is 60% and the absorption strength declines as $\rho(r)$ (lower covering factor and/or optical depth as the gas spreads out to large radius). This model is by no means unique; the essential point is that a model in which the cool gas is accelerated as radius increases, while its density declines with r , can naturally produce an asymmetric line profile with a tail of absorption to high velocities. This shape is similar to the composite spectrum and to the individual absorption lines we detect (Figure 4). The model spectrum does not have gas at velocities as large as observed, which could be due to limitations of the model and our assumptions about σ_h and L_M . This is not a unique model prediction; for example, low column density clouds might be accelerated to higher velocities (see Rupke et al. 2005b), possibly producing a similar profile. Detailed comparisons of wind models and the spectra should be a constraint on wind physics.

Wind velocities that increase with mass and SFR undermine some of the assumptions in models of winds that emphasize blowout in low mass galaxies (e.g. Dekel & Silk 1986). Incorporating wind velocities that increase with mass ($V_{wind} \sim V_{esc}$, rather than constant V_{wind}) into cosmological simulations does a better job of reproducing the IGM enrichment and mass-metallicity relation (Oppenheimer & Davé 2006; Finlator & Davé 2008). Regardless of the energy vs. momentum-driven controversy, we find that indeed $V_{wind} \sim V_{esc}$ (Figures 15 and 16), reinforcing that this is a better scaling to apply.

7.5. Descendants of the DEEP2 sample

Winds have previously been detected in low-redshift dwarf starbursts and IR-luminous galaxies (e.g. Heckman et al.

2000; Martin 2005; Rupke et al. 2005b), in $z \sim 0.6$ luminous post-starbursts (Tremonti et al. 2007), and in $z \sim 3$ Lyman break galaxies (Pettini et al. 2000; Shapley et al. 2003). A common feature of all but the dwarfs is that they have a high fraction of mergers or progenitors of ellipticals; in the case of the $z \sim 3$ galaxies this is based on their clustering (Adelberger et al. 2005). This leaves open the question of whether winds were mostly associated with elliptical formation or were also part of the past of today’s luminous non-starburst spirals. Were outflows driven from massive galaxies only in bursty events associated with mergers or quenching of star formation, or were they also driven during the relatively steady high-SFR mode that governs blue galaxies at $z \sim 1$ (Noeske et al. 2007a)?

The DEEP2 Mg II sample shows that winds are common in the blue cloud of star-forming galaxies at $z \sim 1.4$. Although we are only probing the brightest 1-1.5 mag of galaxies at a given $U - B$ color, the sample spans a wide range of stellar mass and color, showing that winds occur even in low-mass galaxies with $M_* < 10^{10} M_\odot$. These are well below the transition mass for quenching of star formation (Bundy et al. 2006) and are unlikely to evolve quickly onto the red sequence.

Because the DEEP2 Mg II sample is the high-redshift tip of a classical magnitude-selected survey, we can trace the blue population down in redshift. The evolution of the blue cloud in DEEP2 suggests that most of the galaxies stay blue and fade as their SFR declines gradually (Blanton 2006; Willmer et al. 2006; Faber et al. 2007; Noeske et al. 2007a). Some of the brightest blue galaxies may turn red; especially in denser environments. At $z > 1$, some of the brightest blue DEEP2 galaxies are in dense environments (Cooper et al. 2007), and from $z = 1.3$ to $z = 1$, the red fraction in DEEP2 groups increases (Gerke et al. 2007). It is likely that some of the $z \sim 1.4$ DEEP2 blue galaxies will turn into ellipticals in groups. However, much of the sample is in the field; blue galaxies in DEEP2 have high number density and much lower clustering than local early-type galaxies (Coil et al. 2008). The combination of number density and clustering shows that most of them will not evolve into local early-types, similar to the argument made by Conroy et al. (2008) for the descendants of $z \sim 2$ galaxies. Note also that of the galaxies with HST/ACS imaging, the merger fraction was very low, 3/118, while 50/118 were classified as face-on or inclined disk objects (Section 6.2).

An analysis of the clustering and number density of $z \sim 2$ star-forming galaxies indicates that they will evolve mostly into L_* galaxies today, including many massive spirals and some ellipticals (Conroy et al. 2008). The $z \sim 2$ galaxies are roughly intermediate in properties and time between the $z \sim 3$ Lyman break galaxies and the $z \sim 1.4$ DEEP2 galaxies, reinforcing that the DEEP2 Mg II galaxies are most likely to turn into massive spirals like the Milky Way. The lookback time to $z = 1.4$ is 9.0 Gyr, approximately the epoch at which the Milky Way thin disk begins to form (Edvardsson et al. 1993), which could plausibly be associated with a very high SFR.

We conclude that the prevalence of winds in the DEEP2 $z \sim 1.4$ sample shows that many L_* galaxies, including spirals, drove a wind during their early, high-SFR, formative phases. Most blue galaxies continue to form stars down to the present day, which implies that a strong SFR-driven wind does not prevent subsequent star formation.

Winds, possibly from AGN, are a popular mechanism for truncating or quenching further gas accretion and star for-

mation during merger formation of spheroidal galaxies (e.g. Sanders 1988; Cox et al. 2006; Tremonti et al. 2007). The physics of how the energy source couples to the ISM to clear it from the galaxy are not well understood. Galaxy-scale simulations cannot resolve the AGN, and popular models incorporating AGN feedback (e.g. Hopkins et al. 2006) couple the AGN energy directly to the ISM, which could be unrealistically efficient.

It may be that AGN energy input, orbital energy from the merger, or an extremely high SFR (effectively Eddington limited, as in Murray et al. 2005 or Socrates et al. 2006) can clear the ISM from the progenitors of ellipticals, but these have yet to be proven. SFRs like those observed in the DEEP2 $z \sim 1.4$ sample, $10\text{--}50 M_{\odot} \text{yr}^{-1}$, do not appear to remove enough gas to deter subsequent star formation. There is evidence that radiation from QSOs heats and ionizes the IGM out to large distances, as seen in the proximity effect (shown for metal lines by Wild et al. 2008), but also that the effect is anisotropic, weaker in the transverse direction (Hennawi & Prochaska 2007). The physics of QSOs ionizing the ISM or IGM absorbers are understood, but it is more difficult to couple radiation to the gas to transfer momentum and cause blowout, which is a current weakness of the AGN quenching scenario.

8. CONCLUSIONS

We have used 1406 spectra of blue star-forming galaxies at $z \sim 1.4$ in the DEEP2 redshift survey to detect blueshifted Mg II and Mg I absorption in the coadded spectrum, and in a subset of the individual spectra that have high enough S/N. The blueshifted Mg II absorption reaches a depth of 55%, indicating that large-scale wind-driven outflows in cool, low-ionization gas exist in at least half of the galaxies. The convolution of frequency and covering fraction of outflows in low-redshift IR-luminous galaxies is ~ 0.2 (Rupke et al. 2005b). The 55% absorption in our sample suggests that in fact all of the $z \sim 1.4$ star-forming galaxies are driving outflows, and that the Mg II covering fraction is higher than seen in Na I in the local IR-luminous galaxies.

The outflows are driven by star formation; about 50 of the galaxies show narrow Mg II emission indicating AGN activity, but these have a similar outflow signature to the rest. The outflows show an asymmetric absorption profile with a tail to high velocities; the median of the absorption is $\sim -250 \text{ km s}^{-1}$, with absorption at 10% depth out to $\sim -500 \text{ km s}^{-1}$. In the high stellar mass subsample, absorption is visible out to $\sim -1000 \text{ km s}^{-1}$.

The Mg II absorption is quite saturated and the overall covering fraction is large, given the 55% absorption trough. Applying the doublet ratio method to the Mg II doublet, we find that the optical depth is ~ 10 and the column density of the absorbers is $N_H \sim 10^{20}$, possibly even higher given the high optical depths. This implies that a typical luminous star-forming galaxy at $z = 1.4$ is blowing out and covered by a sub-damped Lyman- α absorber.

The sample galaxies have SFRs of $10 - 100 M_{\odot} \text{yr}^{-1}$, derived from UV fluxes and normalized to infrared luminosities; the median galaxy has $L_{IR} = 1.3 \times 10^{11} L_{\odot}$. We find mass outflow rates of order $20 M_{\odot} \text{yr}^{-1}$ using the measured cool gas outflow speed and column density, and a radius of at least 5 kpc, about the optical size of the galaxies. The outflow rate is of the same order as the galaxies' star formation rate, in accord with local starburst wind galaxies and models of

high-redshift chemical evolution. Maintaining both high SFR and high outflow suggests that galaxies process gas relatively quickly and the rates are governed by infall (e.g. Heckman et al. 2000; Erb 2008). Substantial outflows can explain why the baryon fraction in galaxy disks is lower than the global value. The actual radius the outflows can reach is not known; it is possible that these outflows will give rise to Mg II absorption line systems at 20-50 kpc.

We divide the galaxies into subsamples by stellar mass, color, and star formation rate. We find strong blueshifted Mg II absorption in all subsamples, across factors of ~ 30 in stellar mass and ~ 10 in SFR. For 118 of the galaxies, we have HST/ACS imaging and divide the galaxies into types including disks, irregulars and mergers. Again we find outflow absorption in all types. Nearly half of the galaxies are spirals and only 3/118 are obvious mergers. This is distinct from wind samples studied in absorption at lower redshifts, which tend to be either IR-luminous starbursts (Heckman et al. 2000), IR-luminous galaxies with a large merger fraction (Rupke et al. 2005b; Martin 2005), or post-starbursts (Tremonti et al. 2007). The blue galaxy population has a high SFR across all luminous galaxies at $z > 1$ (Noeske et al. 2007a), rather than high SFR confined to a small fraction of the objects, and this places many of the blue galaxies at $z \sim 1.4$ above the $SFR > 0.1 M_{\odot} \text{yr}^{-1} \text{ kpc}^{-2}$ criterion for driving a wind that appears to hold in the local universe (Heckman 2002).

The Mg II outflow absorption is stronger and reaches to larger velocities for high-stellar-mass, high-SFR galaxies. The outflow velocity scales with SFR as $V_{wind} \sim SFR^{0.3}$, similar to the scaling found by Martin (2005) in low-redshift ULIRGs. The outflow velocity scales roughly as the galaxy escape velocities, which we derive from [O II] emission line velocity widths. Although theoretical treatments of galactic winds have tended to emphasize their effect on low-mass galaxies, the velocity scaling we find suggests that gas may be able to escape from high-mass galaxies. A scaling relation of this type should be applied in theoretical models of galaxy formation and IGM evolution (e.g. Finlator & Davé 2008). This velocity scaling may support momentum-driven wind models over energy-driven winds; further study of the wind models and the detailed absorption line profiles should yield insights into the wind physics.

Most of these $z \sim 1.4$ DEEP2 blue star-forming galaxies will evolve into massive L_* galaxies at $z = 0$, including many star-forming spirals, although some fraction will turn into ellipticals. The prevalence of Mg II outflows in this DEEP2 sample thus indicates that winds are not confined to mergers and elliptical progenitors; the progenitors of Milky Way-type galaxies drove winds in the past. Traces of these past winds in high-mass galaxies are likely not visible in the mass-metallicity relation (Dalcanton 2007), but they will have influenced the chemical evolution of the galaxies and the IGM.

Most of the descendants of the blue star-forming galaxies continue to form stars, which implies that the winds in these galaxies are not strong enough to clear the ISM and quench star formation. Powerful winds during galaxy mergers are a popular mechanism for truncating gas accretion and star formation in red galaxies (e.g. Sanders 1988; Cox et al. 2006). These invoke energy input from AGN, orbital energy of the merger, or extremely high star formation rates. The details of how the energy source couples to the ISM to clear it are not well understood. We show that strong star-formation driven winds do not deter subsequent star formation in the blue

galaxy population. Although star-formation driven winds are not expected to clear their hosts' ISM based on their energetics, AGN-driven winds must be consistently stronger and very well coupled to the ISM if they are to explain quenching. The physics of the coupling are a difficult problem that must be understood to make wind quenching scenarios viable.

We are grateful to Christy Tremonti for inspiring this project and much advice, and to Kristian Finlator, Romeel Davé, David Rupke, Sylvain Veilleux and Norman Murray for helpful discussions. We acknowledge the cultural role of the summit of Mauna Kea within the indigenous Hawaiian community and are grateful to have been able to observe from this mountain. BJW has been supported by NASA/Spitzer con-

tract 1255094. ALC is supported by NASA through Hubble Fellowship grant HF-01182.01-A awarded by STScI, which is operated by AURA for NASA under contract NAS 5-26555. DEEP2 has been supported by NSF grants AST05-07428 and AST05-07483. WIRC observations were obtained at the Hale Telescope, Palomar Observatory as part of a continuing collaboration between Caltech, NASA/JPL, and Cornell University. This work is based in part on observations made with the Spitzer Space Telescope operated by and funded through the Jet Propulsion Laboratory, California Institute of Technology under a contract with NASA. Support for this work was provided by NASA through contract 1255094 issued by JPL/Caltech.

Facilities: Keck, Spitzer (MIPS), Hale.

APPENDIX

STELLAR MASSES IN DEEP2 FROM THE COLOR- M/L RELATION

It has been shown for local galaxies that reasonable star formation histories produce a relation between color and stellar M/L (Bell & de Jong 2001). We would like to use such a relation to infer stellar mass M_* for galaxies that do not have K -band data nor stellar masses computed by Bundy et al. (2006). We should not directly apply the local relations (Bell & de Jong 2001; Bell et al. 2003) since higher-redshift galaxies have different star formation histories, so we empirically correct the color- M/L relations using galaxies that do have K -band stellar masses.

We first compute the relation for M_*/L_B as a function of $B - V$ for $z = 0$ galaxies (Bell et al. 2003):

$$\log M/L_B(z=0) = -0.942 + 1.737(B - V_{Vega}), \quad (\text{A1})$$

for a ‘‘diet Salpeter’’ IMF¹⁴ (Bell & de Jong 2001). M_B and $B - V$ are obtained by our K -correction methods.

This color- M/L relation could easily change with redshift. We calibrate the stellar masses by a least-squares fit of a correction term C_K between the color- M/L masses and the K -derived masses of Bundy et al. (2006). We fit to all 11924 galaxies with K and masses in $0 < z < 1.5$, not just the Mg II sample, and find:

$$M_* = L_{B,Vega} \times M/L_B(z=0) \times C_K(U - B, z), \quad (\text{A2})$$

$$\log C_K(U - B, z) = -0.0244 - 0.398z + 0.105(U - B_{Vega}). \quad (\text{A3})$$

Here $U - B_{Vega} = U - B_{AB} - 0.85$ and $B - V_{Vega} = B - V_{AB} + 0.11$. The scatter about the fit is 0.25 dex in stellar mass. This formula with C_K applies to the entire DEEP2 sample over the range $0 < z < 1.5$. There are systematic residual patterns with color and redshift of 0.1 dex (0-to-peak) in the mean, but this is less than the 0.3 dex rms scatter of individual galaxies about the relation. Introducing second-order terms in $U - B$ and z does not improve the residuals significantly.

The corrected stellar masses presented here are on the scale of Bundy et al. (2006), who used a Chabrier IMF. For the 1406-galaxy Mg II sample, 409 have K magnitudes and masses from Bundy et al. (2006). Figure 9 compares the mass estimates from color- M/L to those from K -band, and demonstrates that there is a good correlation, although with significant scatter: the color- M/L masses are 0.09 dex lower with an RMS dispersion of 0.30 dex.

REFERENCES

- Adelberger, K.L., Steidel, C.C., Pettini, M., Shapley, A.E., Reddy, N.A., & Erb, D.K. 2005, ApJ, 619, 697
 Bell, E.F. 2002, ApJ, 577, 150
 Bell, E.F., & de Jong, R.S. 2001, ApJ, 550, 212
 Bell, E.F., McIntosh, D.H., Katz, N., & Weinberg, M.D. 2003, ApJS, 149, 289
 Bell, E.F., et al. 2005, ApJ, 625, 23
 Bergeron, J., & Boissé, P. 1991, A&A, 243, 344
 Bertin, E., & Arnouts, S. 1996, A&AS, 117, 393
 Binney, J. & Tremaine, S. 1987, Galactic Dynamics (Princeton: Princeton U.P.)
 Bland, J., & Tully, B. 1988, Nature, 334, 43
 Blanton, M.R. 2006, ApJ, 648, 268
 Bond, N.A., Churchill, C.W., Charlton, J.C., & Vogt, S.S. 2001, ApJ, 562, 641
 Bouché, N., Murphy, M.T., Péroux, C., Csabai, I., & Wild, V. 2006, MNRAS, 371, 495
 Bowen, D.V., Pettini, M., Penston, M.V., & Blades, C. 1991, MNRAS, 249, 145
 Bowen, D.V., Blades, J.C., & Pettini, M. 1995, ApJ, 448, 634
 Bruzual, G., & Charlot, S. 2003, MNRAS, 344, 1000
 Bundy, K., et al. 2006, ApJ, 651, 120
 Ceverino, D., & Klypin, A. 2007, arXiv:0712.3285
 Charlton, J. C., & Churchill, C. W. 1998, ApJ, 499, 181
 Chen, H.-W., & Tinker, J. L. 2008, arXiv:0801.2169
 Chevalier, R.A., & Clegg, A.W. 1985, Nature, 317, 44

¹⁴ For many typical galaxy SF histories, the ‘‘diet Salpeter’’ IMF implies about 0.15 dex lower mass than a Salpeter IMF, a Kroupa IMF is slightly lower than diet Salpeter, and a Chabrier IMF is 0.2-0.25 dex lower than Salpeter. In practice, for our sample, the main effect of different IMFs is to shift the zeropoints of mass or SFR due to a change in the ratio of high to low mass stars. SFR calibrations are often referenced to the Salpeter IMF (e.g. Kennicutt 1998) or sometimes Kroupa (Bell et al. 2005), while stellar mass estimates often use somewhat lighter IMFs (Bell & de Jong 2001; Bundy et al. 2006). It is vitally important when comparing SFR estimates to compensate for the assumed IMF.

- Coil, A.L., et al. 2004a, *ApJ*, 609, 525
 Coil, A.L., et al. 2008, *ApJ*, 672, 153
 Coil, A.L., Newman, J.A., Kaiser, N., Davis, M., Ma, C.-P., Kocevski, D.D., & Koo, D.C. 2004b, *ApJ*, 617, 765
 Conroy, C., Shapley, A. E., Tinker, J. L., Santos, M. R., & Lemson, G. 2008, *ApJ*, 679, 1192
 Conselice, C.J., Bundy, K., U, V., Eisenhardt, P., Lotz, J., & Newman, J. 2008, *MNRAS*, 383, 1366
 Cooper, M. C., et al. 2007, *MNRAS*, 376, 1445
 Cox, T.J., Di Matteo, T., Hernquist, L., Hopkins, P.F., Robertson, B., & Springel, V. 2006, *ApJ*, 643, 692
 Crenshaw, D. M., Kraemer, S. B., Boggess, A., Maran, S. P., Mushotzky, R. F., & Wu, C.-C. 1999, *ApJ*, 516, 750
 Dalcanton, J.J. 2007, *ApJ*, 658, 941
 Dale, D.A., & Helou, G. 2002, *ApJ*, 576, 159
 Dalla Vecchia, C., & Schaye, J. 2008, *MNRAS*, 387, 1431
 Davis, M. et al. 2003, *Proc. SPIE*, 4834, 161
 Davis, M., et al. 2007, *ApJ*, 660, L1
 Dawson, S., Spinrad, H., Stern, D., Dey, A., van Breugel, W., de Vries, W., & Reuland, M. 2002, *ApJ*, 570, 92
 De Young, D.S., & Heckman, T.M. 1994, *ApJ*, 431, 598
 Dekel, A., & Silk, J. 1986, *ApJ*, 303, 39
 Dubois, Y., & Teyssier, R. 2008, *A&A*, 477, 79
 Dutton, A. A., van den Bosch, F. C., Dekel, A., & Courteau, S. 2007, *ApJ*, 654, 27
 Edvardsson, B., Andersen, J., Gustafsson, B., Lambert, D. L., Nissen, P. E., & Tomkin, J. 1993, *A&A*, 275, 101
 Eisenstein, D.J., et al. 2001, *AJ*, 122, 2267
 Erb, D. K. 2008, *ApJ*, 674, 151
 Faber, S.M., et al. 2007, *ApJ*, 665, 265
 Finlator, K., & Dave, R. 2008, *MNRAS*, 385, 2181
 Fioc, M., & Rocca-Volmerange, B. 1997, *A&A*, 326, 950
 Frye, B., Broadhurst, T., & Benítez, N. 2002, *ApJ*, 568, 558
 Fujita, A., Martin, C.L., Mac Low, M.-M., New, K.C.B., & Weaver, R. 2008, arXiv:0803.2892
 Fukugita, M., Hogan, C.J., & Peebles, P.J.E. 1998, *ApJ*, 503, 518
 Garnett, D.R. 2002, *ApJ*, 581, 1019
 Geha, M., Blanton, M.R., Masjedi, M., & West, A.A. 2006, *ApJ*, 653, 240
 Gerke, B.F., et al. 2007, *MNRAS*, 376, 1425
 Heckman, T. M. 2002, in *Extragalactic Gas at Low Redshift*, 254, 292
 Heckman, T.M., Armus, L., & Miley, G.K. 1990, *ApJS*, 74, 833
 Heckman, T.M., Lehnert, M.D., Strickland, D.K., & Armus, L. 2000, *ApJS*, 129, 493
 Heckman, T.M., Robert, C., Leitherer, C., Garnett, D.R., & van der Rydt, F. 1998, *ApJ*, 503, 646
 Hennawi, J. F., et al. 2006, *ApJ*, 651, 61
 Hennawi, J. F., & Prochaska, J. X. 2007, *ApJ*, 655, 735
 Hopkins, A. 2004, *ApJ*, 615, 209
 Hopkins, P.F., Hernquist, L., Cox, T.J., Di Matteo, T., Robertson, B., & Springel, V. 2006, *ApJS*, 163, 1
 Jenkins, E.B. 1986, *ApJ*, 304, 739
 Kacprzak, G.G., Churchill, C.W., Steidel, C.C., Murphy, M.T., & Evans, J.L. 2007, *ApJ*, 662, 909
 Kennicutt, R.C. 1998, *ARA&A*, 36, 189
 Kewley, L.J., Geller, M.J., & Jansen, R.A. 2004, *AJ*, 127, 2002
 Kinney, A. L., Calzetti, D., Bohlin, R. C., McQuade, K., Storchi-Bergmann, T., & Schmitt, H. R. 1996, *ApJ*, 467, 38
 Kobulnicky, H.A., & Gebhardt, K. 2000, *AJ*, 119, 1608
 Kondo, Y., Modisette, J. L., & Wolf, G. W. 1975, *ApJ*, 199, 110
 Kroupa, P. 2001, *MNRAS*, 322, 231
 Lamers, H.J., van der Hucht, K.A., Snijders, M.A.J., & Sakhbullin, N. 1973, *A&A*, 25, 105
 Lamers, H.J.G.L.M., & Snijders, M. A. J. 1975, *A&A*, 41, 259
 Lanzetta, K.M., & Bowen, D. 1990, *ApJ*, 357, 321
 Larson, R.B. 1974, *MNRAS*, 169, 229
 Le Floch, E. et al. 2005, *ApJ*, 632, 169
 Lehnert, M.D. & Heckman, T.M. 1996, *ApJ*, 462, 651
 Leitherer, C., et al. 1999, *ApJS*, 123, 3
 Lilly, S.J., Le Fevre, O., Hammer, F., & Crampton, D. 1996, *ApJ*, 460, L1
 Lin, L., et al. 2004, *ApJ*, 617, L9
 Lin, L. et al. 2007, *ApJ*, 660, L51
 Lotz, J.M. et al. 2008, *ApJ*, 672, 177
 Mac Low, M.-M., & Ferrara, A. 1999, *ApJ*, 513, 142
 Martin, C.L. 1999, *ApJ*, 513, 156
 Martin, C.L. 2005, *ApJ*, 621, 227
 Martin, C.L. 2006, *ApJ*, 647, 222
 Ménard, B., & Chelouche, D. 2008, arXiv:0803.0745
 Meurer, G.R., Heckman, T.M., & Calzetti, D. 1999, *ApJ*, 521, 64
 Mirabel, I.F. & Sanders, D.B. 1988, *ApJ*, 335, 104
 Mo, H.J., & Mao, S. 2004, *MNRAS*, 353, 829
 Morganti, R., Tadhunter, C. N., & Oosterloo, T. A. 2005, *A&A*, 444, L9
 Moustakas, J., Kennicutt, R.C., & Tremonti, C.A. 2006, *ApJ*, 642, 775
 Murray, N., Martin, C.L., Quataert, E., & Thompson, T.A. 2007, *ApJ*, 660, 211
 Murray, N., Quataert, E., & Thompson, T.A. 2005, *ApJ*, 618, 569
 Nandra, K. et al. 2007, *ApJ*, 660, L11
 Nestor, D. B., Turnshek, D. A., & Rao, S. M. 2005, *ApJ*, 628, 637
 Nesvadba, N. P. H., Lehnert, M. D., Eisenhauer, F., Gilbert, A., Tecza, M., & Abuter, R. 2006, *ApJ*, 650, 693
 Noeske, K.G. et al. 2007a, *ApJ*, 660, L43
 Noeske, K.G., et al. 2007b, *ApJ*, 660, L47
 Oppenheimer, B.D., & Davé, R. 2006, *MNRAS*, 373, 1265
 Papovich, C. et al. 2007, *ApJ*, submitted
 Pettini, M., Steidel, C.C., Adelberger, K.L., Dickinson, M., & Giavalisco, M. 2000, *ApJ*, 528, 96
 Pettini, M., Rix, S.A., Steidel, C.C., Adelberger, K.L., Hunt, M.P., & Shapley, A.E. 2002, *ApJ*, 569, 742
 Phillips, A.C. 1993, *AJ*, 105, 486
 Praderie, F., Talavera, A., & Lamers, H.J.G.L.M. 1980, *A&A*, 86, 271
 Rieke, G.H., et al. 2004, *ApJS*, 154, 25
 Rigby, J. R., et al. 2008, *ApJ*, 675, 262
 Rix, H., Guhathakurta, P., Colless, M., & Ing, K. 1997, *MNRAS*, 285, 779
 Rodríguez-Merino, L. H., Chavez, M., Bertone, E., & Buzzoni, A. 2005, *ApJ*, 626, 411
 Rupke, D.S., & Veilleux, S. 2005, *ApJ*, 631, L37
 Rupke, D.S., Veilleux, S., & Sanders, D.B. 2005a, *ApJS*, 160, 87
 Rupke, D.S., Veilleux, S., & Sanders, D.B. 2005b, *ApJS*, 160, 115
 Rupke, D.S., Veilleux, S., & Sanders, D.B. 2005c, *ApJ*, 632, 751
 Salim, S. et al. 2007, *ApJS*, 173, 267
 Sato, T. et al. 2008, *ApJ*, submitted, arXiv:0804.4312
 Savage, B.D. & Sembach, K. 1996, *ARA&A* 34, 279
 Sawicki, M. et al. 2008, *ApJ*, submitted
 Scannapieco, E., & Oh, S. P. 2004, *ApJ*, 608, 62
 Schwartz, C.M., & Martin, C.L. 2004, *ApJ*, 610, 201
 Schwartz, C.M., Martin, C.L., Chandar, R., Leitherer, C., Heckman, T.M., & Oey, M.S. 2006, *ApJ*, 646, 858
 Seibert, M., et al. 2005, *ApJ*, 619, L55
 Shapley, A.E., Steidel, C.C., Pettini, M., & Adelberger, K.L. 2003, *ApJ*, 588, 65
 Shapley, A.E., Coil, A.L., Ma, C.-P., & Bundy, K. 2005, *ApJ*, 635, 1006
 Snow, T.P., Lamers, H.J.G.L.M., Lindholm, D.M., & Odell, A.P. 1994, *ApJS*, 95, 163
 Socrates, A., Davis, S. W., & Ramirez-Ruiz, E. 2006, arXiv:astro-ph/0609796
 Somerville, R. S., & Primack, J. R. 1999, *MNRAS*, 310, 1087
 Spitzer, L. 1968, *Diffuse Matter in Space* (New York: Wiley-Interscience)
 Steidel, C.C., Dickinson, M., & Persson, S.E. 1994, *ApJ*, 437, L75
 Steidel, C.C., Kollmeier, J.A., Shapley, A.E., Churchill, C.W., Dickinson, M., & Pettini, M. 2002, *ApJ*, 570, 526

- Steidel, C. C., & Sargent, W. L. W. 1992, *ApJS*, 80, 1
- Strickland, D.K., Heckman, T.M., Colbert, E.J.M., Hoopes, C.G., & Weaver, K.A. 2004, *ApJS*, 151, 193
- Strickland, D. K., & Stevens, I. R. 2000, *MNRAS*, 314, 511
- Thacker, R. J., Scannapieco, E., & Couchman, H. M. P. 2006, *ApJ*, 653, 86
- Tinker, J. L., & Chen, H.-W. 2008, *ApJ*, 679, 1218
- Tremonti, C.A., et al. 2004, *ApJ*, 613, 898
- Tremonti, C.A., Moustakas, J., & Diamond-Stanic, A.M. 2007, *ApJ*, 663, L77
- Treyer, M. et al. 2007, *ApJS*, 173, 256
- Trump, J.R., et al. 2006, *ApJS*, 165, 1
- Veilleux, S., Cecil, G., & Bland-Hawthorn, J. 2005, *ARA&A*, 43, 769
- Verdugo, E., Talavera, A., & Gómez de Castro, A.I. 1999, *A&AS*, 137, 351
- Weiner, B.J., et al. 2005, *ApJ*, 620, 595
- Weiner, B.J., et al. 2006, *ApJ*, 653, 1027
- Weiner, B.J., et al. 2007, *ApJ*, 660, L39
- Wild, V., Hewett, P. C., & Pettini, M. 2006, *MNRAS*, 367, 211
- Wild, V., et al. 2008, *MNRAS*, 388, 227
- Willmer, C.N.A., et al. 2006, *ApJ*, 647, 853
- Wu, C.-C., Boggess, A., & Gull, T.R. 1983, *ApJ*, 266, 28
- Zibetti, S., Ménard, B., Nestor, D.B., Quider, A.M., Rao, S.M., & Turnshek, D.A. 2007, *ApJ*, 658, 161